Quantification of Blood Flow Based on Color Doppler Echocardiography

著者	Sri Oktamuliani
学位授与機関	Tohoku University
学位授与番号	11301甲第18968号
URL	http://hdl.handle.net/10097/00129826

Quantification of Blood Flow Based on Color Doppler Echocardiography

Sri Oktamuliani
Graduate School of Biomedical Engineering
Tohoku University

A dissertation submitted in partial fulfillment for the degree of Doctor of Philosophy

2019

Declaration of Authorship

I, SRI OKTAMULIANI, declare that this dissertation titled, 'QUANTIFICATION OF BLOOD FLOW BASED ON COLOR DOPPLER ECHOCARDIOGRAPHY' and the work presented in it are my own. I confirm that:

- This work was done wholly or mainly while in candidature for a research degree at this University.
- Where any part of this dissertation has previously been submitted for a degree or any other qualification at this University or any other institution, this has been clearly stated.
- Where I have consulted the published work of others, this is always clearly attributed.
- Where I have quoted from the work of others, the source is always given. With the exception of such quotations, this dissertation is entirely my own work.
- I have acknowledged all main sources of help.
- Where the dissertation is based on work done by myself jointly with others, I have made clear exactly what was done by others and what I have contributed myself.

Signed: _____

Date: _____

"Laa hawla wa laa quwatta illa billah. There is no power and no strength except with ALLAH"

The Prophet, Muhammad Sallallahu Alaihi Wassalam

TOHOKU UNIVERSITY

Abstract

Graduate School of Biomedical Engineering

Doctor of Philosophy

by Sri Oktamuliani

Quantitative evaluation of blood flow contributes to diagnosis and prognosis of cardiac function. In the present study, two-dimensional blood flow visualization algorithm named Echodynamography (EDG) based on color Doppler echocardiography data and fluid dynamic theories was developed for quantitative analysis of blood flow. Virtual color Doppler image; generated from particle image velocimetry (PIV) data of heart phantom, was analyzed by EDG and the result was compared with the original PIV velocity for validation of the EDG method. The correlation was very strong (r^2= 0.99) in the velocity component along the ultrasonic beam and moderate in the perpendicular direction. In the clinical setting, six healthy volunteers, eight patients with aortic stenosis (AS), and seven patients with myocardial infarction (MI) were enrolled for EDG study. Hemodynamic parameters such as vortex strength, vortex sphericity index and Reynolds number were compared in all groups. The vortex strength (healthy: 3.09±2.06 vs. AS: 5.36±2.81 (p<0.0001) vs. MI: 3.32±2.28 (p=0.184)), vortex sphericity index (healthy: 0.51±0.22 vs. AS: 0.99±0.44 (p<0.0001) vs. MI: 0.60±0.27 (p=0.626)) and Reynolds number (healthy: 1020±603 vs. AS: 2405±1562 (p<0.0001) vs. MI: 1290±913 (p=0.137) showed significant difference in the pairs. Reynolds number showed positive correlation with the vortex strength (healthy: r=0.79, p=0.29, AS: r=0.98, p<0.001, MI: r=0.85, p<0.033) and vortex sphericity index (healthy: r=0.21, p<0.001, AS: r=0.47, p<0.001, MI: r=0.47, p<0.001). Quantitative blood flow analysis by EDG especially focusing on intraventricular vortex is important to assess cardiac function.

keyword: Echodynamography, blood flow, velocity vectors, left ventricular.

和文アブストラクト

血流の定量的解析は心機能の診断と予後予測に寄与する。本研究ではカラードプラ心エコーデータに流体力学の諸法則を応用してEchodynamography (EDG)と名付けた2次元血流表示方法を開発した。心臓モデルにおけるparticle image velocimetry (PIV)データをカラードプラに変換したバーチャルカラードプラデータをEDGに代入し、結果を元データと比較してEDGの妥当性評価を行った。超音波ビームに沿う方向の速度成分では相関は非常に高く(r^2= 0.99)、ビームに垂直な方向の速度成分でも有意な相関 (r2=0.44) が認められた。臨床において正常者 (Norm) 6名、大動脈弁狭窄症 (AS) 8名、心筋梗塞 (MI) 7名についてEDGによる血流解析を行った。血流パラメータとしてvortex strength、vortex sphericity、Reynolds numberなどを計測し各群間で比較した。Vortex strength (Norm: 3.09±2.06 vs. AS: 5.36±2.81 (p<0.0001) vs. MI: 3.32±2.28 (p=0.184)), vortex sphericity index (Norm: 0.51±0.22 vs. AS: 0.99±0.44 (p<0.0001) vs. MI: 0.60±0.27 (p=0.626)) およびReynolds number (Norm: 1020±603 vs. AS: 2405±1562 (p<0.0001) vs. MI: 1290±913 (p=0.137) とNormとAS群間に有意差を認めた。 Reynolds numberは vortex strength (healthy: r=0.79, p=0.29, AS: r=0.98, p<0.001, MI: r=0.85, p=0.033) およびvortex sphericity index (healthy: r=0.21, p<0.001, AS: r=0.47, p<0.001, MI: r=0.47, p<0.001) のいずれとも有意な相関を示した。EDGによる定量的血流解析、特に心腔内の渦の解析は心機能の解析に重要な情報をもたらす。

Acknowledgements

First of all, I would like to express my very great appreciation to my supervisors Professor Yoshifumi Saijo for his guidance and support. It is tough to express in just a few words all Saijo sensei has done for me. He has been a permanent source of encouragement, motivation, and advice; I guess what I appreciate most is that he has trusted my judgment and has given me the freedom to develop my own ideas. He gave me the chance to come to Japan when I was only a lecturer at Jambi University, for what I am deeply grateful.

My special thanks are extended to the staff of the Graduate School of Biomedical Engineering, in particular, Ms. Haruko Watanabe and Ms. Hiromi Wakabayashi, who have helped me a lot during these years. In my time in the Graduate School of Biomedical Engineering, Tohoku University, I have been lucky enough to meet a good number of great people to share research pain and glories with. During my Ph.D., I had opportunities to be in the clinic of Tohoku medical and pharmaceutical hospital. I would like to offer my special thanks to Dr. Kaoru Hasegawa, my intern medical buddy who always help me give a new data from hospital and Minagawa-sensei for the clinical support and advice.

I am particularly grateful for the assistance given by Syahril Siregar,Ph.D. for his guidance knowing Japanese culture and let his self-discussed about my research, by Mr. So Yaegashi as a tutor for his helping prepare all document for living in Japan. I would also like to thank Mr. Naoya Tsugita for sharing knowledge in the computational study and to Ms. Moe Maeda for her helping during the experimental research, to all members of Saijo laboratory such as Mr. Naoya Kanno, Mr. Ryo Shintate, Dr. Israr Ul Haq, Ms. Rebecca Plant, Mr. Norma Hermawan for their support and kindness.

I would like to offer my special thanks to BUDI-LN (DIKTI and LPDP) for their support systems, allowing me to study in Japan. I owe my deepest gratitude to Dr.techn. Marzuki, Prof. Dr. Zaki Su'ud, M.Eng., and Prof. Sutrisno, M.Sc, Ph.D., who had given the recommendation letter for continuing doctoral study. I would also like to thank Jubaidah, S.Pd., M.Si., from Waseda University for always having her doors open to me, to Rahma Nurkomariah from Kyoto University for her support at the beginning and the end of Ph.D. life, to all warrior of BUDI-LN, who always help each other even we only connect via WhatsApp. These past

three years have been a fantastic period of my life not only professionally, but also personally. I had the opportunity to travel to a lot to conferences and meetings. In those travels, I have met fascinating people with whom I have exchanged ideas, points of view, and also sight-seeing, breathtaking views, and good food and drink. I would like to thank Nagamachi-squad, Yagiyama genks, all members of KMIS, and all members of PPIS for a great time in Sendai.

I do not forget my childhood friends from Painan, my hometown, who have been a best friend ever. I can still call them my friends after all these years, and all these kilometers deserved the most enormous gratitude: Drg. Nesa Perdana Putri, Reski Helfindo, S.E., Myveela Rustam, S.E., Ulfa Golnarsih, A.md.Keb, Ayu Ratna Sari, S.I.P., Chindy Angeline Reviona, S.Pd., Vina Suci Afriyeti, S.H., Ivony Septia Ningsih, S.Pd., Sevriya Amban Suri A.md., Revina Bayu Putri, S.Ikom, Tivony Yunisa, S.Pd., Chika Desvialora, S.T., Erviyulia Faisal, A.md.KL, all the Botak-botak members, Thanks for being there.

I would like to finish by thanking my family because none of this would have been possible without them. Thanks to my sister Syafridawati, S.H., and her Family's, my brother Harry Hazari, A.md., S.Pd., and his Family's for their support and encouragement; and thanks to my parent papa Syofran and mama Arjusneti, for their love, patience, understanding and for following me to the end of the world.

Last, I would like to thank you for reading my dissertation. I guess that when one puts the soul on her work, some of it remains forever imprinted, and flow back to every reader, and there cannot be a more beautiful reward.

Sri Oktamuliani, Sept 2019.

Contents

List of Figures

List of Tables

Abbreviations

1D	**O**ne **D**imensional
2D	**T**wo **D**imensional
3D	**T**hree **D**imensional
AC	**A**trial **C**ontraction
AO	**Ao**rtic
AS	**A**ortic **S**tenosis
A3C	**A**pical **T**hree **C**hamber
BART	**B**lue **A**way **R**ed **T**oward
BME	**B**io**m**edical **E**ngineering
B-Mode	**B**rightness **M**ode
CDE	**C**olor **D**oppler **E**chocardiography
CT	**C**omputed **T**omography
DMSO	**D**i**m**ethyl **S**ulf**o**xide
ECG	**E**lectro**c**ardio**g**ram
EDG	**E**cho**d**ynamo**g**raphy
IHD	**I**schemic **H**eart **D**isease
Is	**I**ndex of **S**phericity
IVC	**I**so**v**olumetric **C**ontraction
IVR	**I**so**v**olumetric **R**elaxation
LA	**L**eft **A**trium
LV	**L**eft **V**entricular
MFAL	**M**ain **F**low **A**xis **L**ine
MI	**M**yocardial **I**nfarction
MRI	**M**agnetic **R**esonance **I**maging

PC-MRA	**P**hase **C**ontrast **M**agnetic **R**esonance **A**ngiography
PIV	**P**article **I**mage **V**elocimetry
PW	**P**ulse **W**ave
PVA	**P**oly**v**inyl **A**lcohol
RA	**R**ight **A**trium
RGB	**R**ed **G**reen **B**lue
ROI	**R**egion **o**f **I**nterest
RV	**R**ight **V**entricular
VE	**V**entricular **E**jection
VF	**V**entricular **F**illing
VFM	**V**ector **F**low **M**apping

Physical Constants

Speed of sound	C	=	$1550m/s$
Kinematic viscosity of blood	ν	=	$3.454 \times 10^{-6}\ m^2/s$
Blood flow density	ρ	=	$1.05 \times 10^3\ \mathrm{kgm}^{-3}$

Symbols

a	cross-sectional vortex latitude
b	cross-sectional vortex longitude
de	diameter equivalent
E_{tot}	point wise error
F_c	Flux flow
F_D	Doppler shift
F_R	reflected ultrasound
F_T	trasmitted ultrasound
j	integer multiplier
k	separation coefficient
L	cross section
P	approximate ellipse
Re	Reynolds number
u_r	Doppler velocity or longitudinal velocity
u_θ	transverse velocity or velocity in perpendicular direction
u_{vr}	vortex flow in radial direction
$u_{v\theta}$	vortex flow in perpendicular direction
u_{br}	base flow in radial direction
$u_{b\theta}$	base flow in perpendicular direction
u_{rPIV}	longitudinal velocity of PIV
$u_{\theta PIV}$	transverse velocity of PIV
$u_{\theta EDG}$	transverse velocity reconstructed
V_o	radial velocity observed

V_t	radial velocity has been changed
V	peak velocity of vortex
V_{max}	Nyquist velocity
$\bar{v}$	velocity
Γ	circulation
ϵ	error point
κ	scaling factor
ν	kinematic viscosity
ξ	weight coefficient
ρ	fluid density
ϕ	Doppler irradiation angle
ψ	stream function
ψ_n	vortex index n
ω	vorticity
∇	nabla

This dissertation is dedicated to my mother, Arjusneti,

my father, Syofran,

my Sister, Syafridawati,
and my brother, Harry Hazari.

Chapter 1

Introduction

The work presented in this document is focused on estimation and visualization of two-dimensional blood flow velocity vectors inside a cardiac of left ventricular by echocardiography that would provide diagnostic and prognostic information on the cardiovascular system and is submitted in partial fulfillment of the requirements for the degree of Doctor of Philosophy of the Tohoku University. This chapter provides a background of the study, the objectives pursued and the structure of the dissertation.

1.1 Background

Biomedical Engineering (BME) is the subject of engineering principles and design concepts to medicine and biology for health care purpose (e.g., diagnostic or therapeutic) [1]. Cardiophysics is an interdisciplinary science that connects the

junction of cardiology and medical physics, with researchers using the method of and theories from physics to study the cardiovascular system.

Cardiovascular disease, especially ischemic heart disease (IHD) is the leading cause of death in the world [2]. In Japan, heart disease is the second leading cause of death. Heart failure is the leading cause of death from heart disease; it is estimated that 1.0 million individuals have heart failure [3]. However, the number of Japanese outpatients with left ventricular (LV) dysfunction is predicted to gain to 1.3 million by 2030 [4] gradually. Besides IHD, an aortic valvular disease caused by atherosclerosis increased in the aging societies, and appropriate treatment of heart failure becomes essential.

The development of cardiovascular imaging is an essential resource for cardiologist and researchers to understand the cardiac morphology, physiology, and pathology [5]. There exist several well-established non-invasive modalities for morphological imaging of heart and vessel, e.g., Echocardiography, Magnetic Resonance Imaging (MRI), and Computed Tomography (CT) [6]. Phase-contrast magnetic resonance angiography (PCMRA) has been used for visualization of 2D and 3D blood flow [7]. However, MRI is an expensive imaging modality, and longtime data acquisition [8].

On the other hands, methods with echocardiography were a simple, portable, non-invasive, and real-time method, which has been an increasing interest technique to image cardiovascular flow. Echocardiography is nearly always the first imaging modality used for cardiac diagnosis (in term of several exams and availability of the equipment). Doppler echocardiography techniques are very widely used and are

part of the standard routine for blood flow measurements [9, 10]. Heart function is to pump blood to all organs; indeed, a heart which might be morphologically different from a healthy heart can still be a functional heart when it delivers the blood to the body. Blood flow analysis of LV may play an essential role in the evaluation of cardiac function besides the classical wall motion analysis. Unfortunately, Doppler echocardiography as a tool to obtain intracardiac flow information has significant limitations; in particular, the only component of the velocity aligned with the ultrasound beam can be measured and does not provide quantitative information. As a result, Doppler measurements may not provide adequate information for either the reconstructive of velocity vector distribution.

Blood flow visualization studies provide clues to reveal physiological and patho-physiological mechanisms potentially allows for prognosis and diagnosis of cardiac function. Recently, visualization methods of 2D blood flow vectors have been proposed by echocardiographic particle image velocimetry (echo-PIV) [11–13] and vector flow mapping (VFM) [14, 15]. Ultrasound contrast agents are injected, and the particle in LV is tracked to visualize 2D blood flow in echo-PIV. Blood flow velocity component in the axis parallel to the ultrasonic beam is measured by Doppler ultrasound, and the perpendicular component is applied from LV wall motion obtained with speckle tracking of the B-mode image in VFM.

Echodynamography (EDG) is also a flow visualization method based on color Doppler echocardiography (CDE) to obtain 2D blood flow vector [16–18]. Blood flow on the observed by color Doppler echocardiography are divided into two flow components. One is "base flow," and the other is "vortex flow." The base flow

comes in from another plane and goes out into another plane. The vortex flow terminates within the observation plane to form a vortex. Newly proposed "flow function" which applies to 3D blood flow is applied to the base flow and "stream function" which is a classical theory in fluid dynamics is applied to vortex flow to obtain blood flow vectors. 2D blood flow vector is obtained without wall motion information in EDG. Thus, EDG is independent of the information of wall motion where VFM is not independent of wall motion [19–21].

1.2 Objectives

In the typical two dimensional (2D) echocardiography image, imaging of the blood flow is possible with Doppler ultrasound. The clinical applications of Doppler ultrasound are numerous and very important for the understanding of the circulation physiology and the evaluation of cardiovascular hemodynamics. Doppler ultrasound has been widely used as a simple and useful tool.

Multi-view approaches have been investigated to overcome this significant limitation of Doppler measurements. In this dissertation, to main research objective have been investigated:

1. Reconstructed color Doppler echocardiography with applying image processing algorithm.

2. Estimated and visualized two-dimensional flow velocity vectors and evaluated hemodynamic parameters based on fluid dynamic theories applied to color Doppler echocardiography.

3. Validated two-dimensional blood flow algorithm using virtual color Doppler of the phantom left ventricle obtained by particle image velocimetry.

4. Explored the potential of two-dimensional blood flow algorithm for *in vivo* application.

1.3 Summary of the Dissertation

This dissertation is structured in 6 chapters. Chapter 1 describe the technical background and objectives. Then, chapter 2 describes the literature review of color Doppler echocardiography systems.

The original work of this dissertation is described in chapter 3, 4, and 5, where methods for the 2D blood flow velocity reconstruction, hemodynamic quantitative, particle image velocimetry validate studies, and clinical application of two-dimensional blood flow are proposed. Last, chapter 6 summaries the main points of this dissertation, putting the original contribution into context and covering the technical implications of the developed methods. In the next paragraph, the contents of each chapter are described one by one.

Chapter 2 describes the clinical context of the research carried out in this dissertation. Physics of echocardiography and color Doppler echocardiography are

summarized. Then it was highlighting the clinical aspects of left ventricle blood flow and cardiac function.

Chapter 3 is the chapter which contains the original contributions of this dissertation. This chapter describes a novel technique to recover a 2D velocity field from 1D velocity along the transducer beam. Studies the applicability of the 2D blood flow velocity described left ventricle vortex flow, vorticity, and main flow axis line.

Chapter 4 provides comprehensive validation studies of 2D blood flow velocity algorithm by particle image velocimetry.

Chapter 5 clinical implication of 2D blood flow applied to healthy participants, aortic stenosis patients, and myocardial infarction patients.

Chapter 6 summaries the main conclusion of this work, and puts into context the original contributions. The future research directions and the technical and clinical implication of the developed techniques are also discussed.

Chapter 2

Literature Review

In this chapter, the principle of Doppler ultrasound and color Doppler echocardiography will be discussed. The dynamics of blood flow in left ventricular during the cardiac cycle is very important to differentiate the normal and abnormal hearts such as aortic stenosis and myocardial infarction.

2.1 Principle of Doppler Ultrasound

Ultrasound refers to sound waves with high frequencies upper audible limit of human hearing. Sound waves are mechanical vibrations by the movement of energy traveling through a medium that can be described in term of frequency or Hertz (Hz, the number of repetitions or cycles per second). Medical ultrasound imaging typically works sound waves at frequencies of 1,000,000 to 2,000,000 Hz (1.0 to 2.0 MHz). In contrast, the human auditory spectrum comprises frequencies between 20 and 20,000 Hz.

Understanding the Doppler principle is began for understanding the color Doppler echocardiography. The first description of the physical principles used in Doppler ultrasound is attributed to Johann Christian Doppler (1803 - 1853), an Austrian mathematician, and scientist who lived in the first half of the 19th century. He proposed a Doppler effect. The Doppler effect is the phenomenon in which the frequency of sound becomes higher when the sound source is approaching the observer, and the frequency become lower when the sound source goes away [Fig.2.1]. By comparing the difference between the signal sent of transmitted ultrasound (F_o) and the signal received of backscattered reflected ultrasound (F_r) could determine a shift (change) in frequency (F_D):

$$Doppler\ shift\ (F_D) = F_r - F_o. \tag{2.1}$$

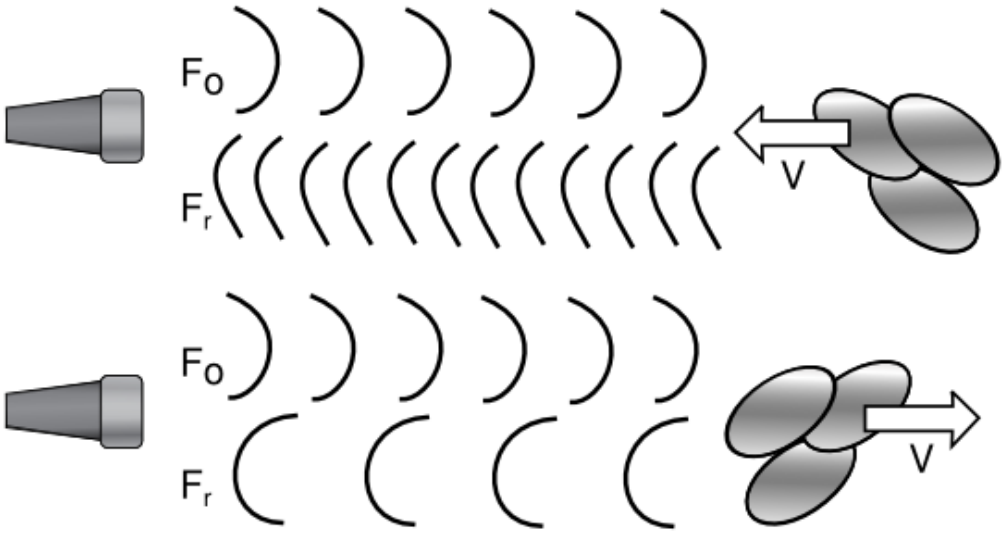

FIGURE 2.1: If the target moves toward the ultrasound transducer, the Doppler shift is positive, and the backscattered (reflected) frequency (F_r) will be higher. If the target moves away from the ultrasound transducer, the Doppler shift is negative, and the backscattered (reflected) frequency (F_r) will be lower.

Doppler ultrasound is based on the change the frequency of the backscatter from

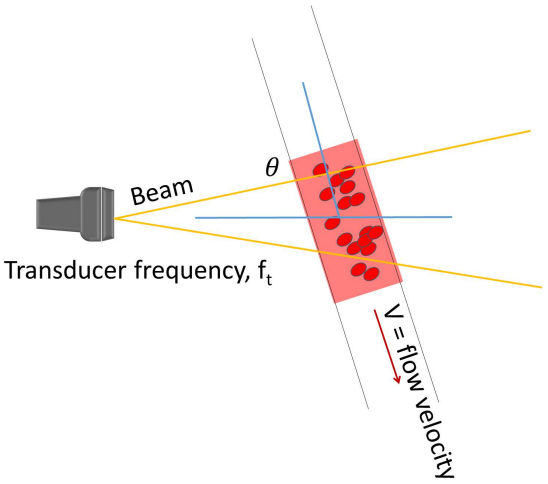

FIGURE 2.2: Doppler ultrasound measures the movement of scatterers through the beam as a phase change in the received signal. If the beam angle is known, measuring velocity can use the result of Doppler frequency.

the red blood cells intercepted by ultrasound [22]. Doppler effect of ultrasound is a method by which one can detect flow in the vessel, identify the direction, measure the velocity of blood flow, and detect the type of flow. The velocity of blood cells can determine by measuring the magnitude of the frequency shift (f_D). Doppler formula as following:

$$u_r = \frac{F_D \; C}{2 \; F_o \; \cos(\phi)} \tag{2.2}$$

where u_r is blood flow velocity (m/s), C is sound propagation velocity (1550 m/s), and ϕ is doppler irradiation angle. The angle of insonation ($\cos\phi$) greatly influences measurements. The more perpendicular the ultrasound beam is the more measurement error. Therefore, take care to align the ultrasound beam as parallel to blood flow as possible [Fig.2.2].

Ultrasound transducer uses piezoelectric crystals to both generate and receive waves. The reflected ultrasound wave impacts the piezoelectric crystal. Thus an

electric current is generated. Image formation is based upon the time interval between ultrasound transmission and the arrival of the reflected signal which related to the distance of a structure from the transducer. Enhancement of spatial resolution was permitted by imaging with higher frequency (and lower wavelength) transducers. However, the depth of tissue penetration or the ability to transmit sufficient ultrasonic energy into the chest is directly related to wavelength and transducer frequency. As a result, the trade-off for the use of higher frequency transducers is reduced tissue penetration.

Image resolution with 2D ultrasound image can be considered in terms of axial, lateral, and elevational resolution. The axial resolution is resolution along the length of the ultrasound beam, depending on the transducer frequency, bandwidth, and pulse length. Lateral resolution is resolution perpendicular to the ultrasound beam, which varies with transducer frequency, aperture (width) of the transducer, beamwidth, bandwidth, and side lobes. Elevational is resolution across the thickness that includes reflected and backscattered signals.

There are several Doppler methods used for cardiac evaluation: continuous wave, pulsed wave, and color flow. Continuous-wave Doppler utilizes two dedicated ultrasound crystals: one for continuous transmission and a second for continuous reception of ultrasound signals that permits measurement of very high-frequency Doppler shifts or velocities. In contrast to continuous-wave Doppler, pulsed wave Doppler permits sampling of local blood flow velocities at a specific region (or sample volume) which records signal along the entire length of the ultrasound beam. Doppler color flow imaging is based upon the principles of pulsed-wave

Doppler. Along each scan line, a pulse of ultrasound is transmitted, and the backscattered signals are then received from each "gate" or sample volume along each line. In order to calculate accurate velocity data, several bursts along each scan line are used, known as the burst length.

2.2 Color Doppler Echocardiography

Ultrasonography of the heart (echocardiography) is one of the widest equipment for diagnosing heart disorders because it provides excellent images, non-invasive, harmless, and relatively inexpensive. Echocardiography provides the ability to detect abnormalities in heart wall motion and diagnostic tool in the critically ill patient's assessment.

Color Doppler echocardiography (CDE) uses Doppler ultrasound to create images of the heart. Ultrasound consists of mechanical waves with frequencies above the upper auditory limit of the 20 kHz. Medical ultrasound devices use longitudinal waves with a frequency range of about 2 - 15 MHz. Adult echocardiography typically uses frequencies of 2 to 7 MHz [23]. The frequency used by the ultrasound transducer affects image resolution and tissue penetration; the higher resolution image, the lower tissue penetration, and vice versa. Moreover, CDE is completed by echocardiogram, the graphic outline of the heart movement, that helps derived the cardiac cycle.

CDE is a method for detecting the location, velocity of moving blood within the heart, and flow pattern, e.g., laminar versus turbulent flow, by displaying blood

flow as color-coded velocities superimposed in real-time on two-dimensional (2D) of M-mode image. Figure 2.3 show apical three-chamber (A3C) view by placing the transducer on the apex of the heart. This plane passes through the apex and the center of the mitral and aortic valves. Although intracardiac flow is known to be 3D, investigated possibility out of plane velocity component are small in-plane corresponding to the echo A3C view. We thus assumed that the main flow arrangement remains measurable in the A3C view without significant loss of information.

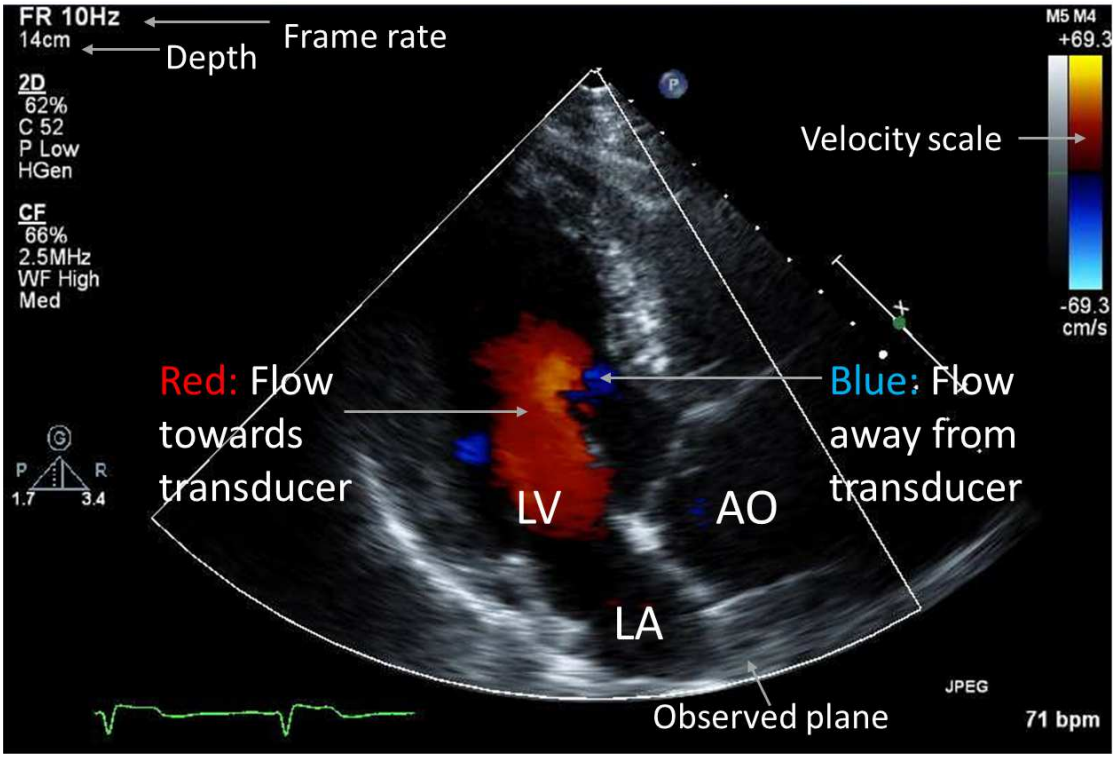

FIGURE 2.3: Color flow Doppler map superimposed on B-mode two-dimensional image of apical three-chamber [Left ventricle (LV), Left atrium (LA) and Aorta (AO)] view. The monochrome image shows a section of heart structure, and color shows the blood flow. Color flow Doppler convention "BART" scale: Blue Away, Red Toward. A red component shows the blood flow approaching the transducer, and a blue component shows the blood flow away from the transducer according to the velocity scale corresponding to the color bar.

CDE is a pulse-wave (PW) Doppler-based technique that displays blood flow velocities as real-time color flow patterns mapped within the cardiac chamber. However, its processing differs from that used to provide the Doppler sonogram. CDE may have to produce several thousand color points of flow information for each frame superimposed on the B-mode image. The transducer is shifted rapidly between B-mode and color flow imaging to give an impression of a combined simultaneous image. The pulses used for color flow imaging usually are three to four times longer than those for the B-mode image, with a corresponding loss of axial resolution.

PW allows for the determination of flow velocity at a specific point (sample volume). The frequency shift is displayed as a color pixel. Conceptually, this can be expressed as a type of "color angiogram." By convention, the blood flow direction in which the speed is displayed using the "BART" (Blue Away Red Toward) scale, with flow toward the transducer typically displayed in color-coded orange/red and flow away from the transducer displayed in color-code blue. A change in hue or lightness interprets the blood flow velocity. Lighter shades are assigned higher velocities within the Nyquist limit.

PW repeatedly samples the returning signal so that the maximum limit to the frequency shift or velocity that can be measured unambiguously. Correct identification of the frequency of an ultrasound waveform requires sampling at least twice per wavelength. Thus, the maximum detectable frequency shift or the Nyquist limit is one-half the PRF. At the Nyquist limit, and each multiple of the limit, aliasing is depicted as color reversal [Fig. 2.4].

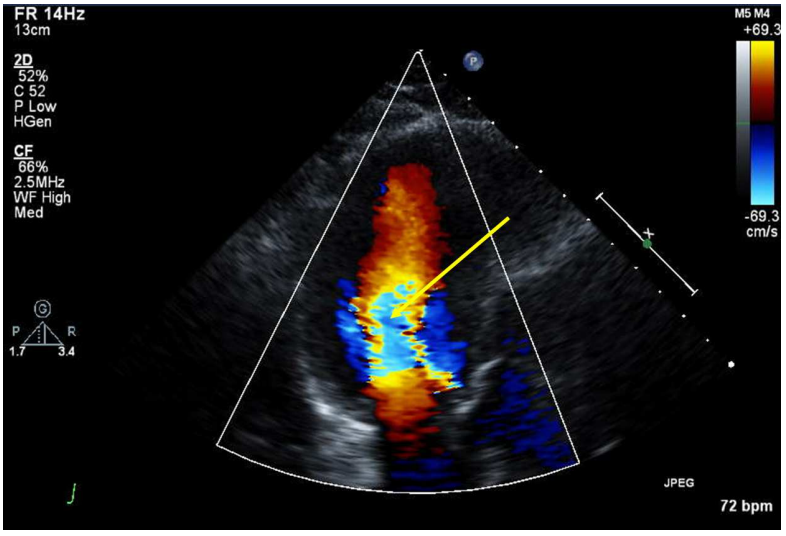

FIGURE 2.4: Aliasing of color doppler imaging. Color image displays regions of aliased flow (yellow arrows).

In general, the active color scan sector should be made as small as is necessary to increase the frame rate and reduce aliasing. Higher frame rates lead to better temporal resolution but may sacrifice image quality and vice versa. Color aliasing occurs even at average intracardiac flow rates that are assigned higher velocities within the Nyquist limit. In this case, however, aliasing appears as color reversal, where flow blue switches to yellow-red, and vice versa. Various blood velocities and directions characterize the turbulent flow. The variance of velocities within jets is usually color-coded as a multicolored mosaic display.

2.3 Dynamics of Left Ventricular Blood Flow

The cardiovascular system is a network consisting of heart, blood vessels, and blood. The heart is four-chambered that act as a pump that consists of the left ventricle (LV), right ventricle (RV), left atrium (LA), and right atrium (RA). The LV is largest and thickest of the heart's chambers where is located in the bottom

left portion of the heart that obtains blood from the LA through the mitral valve and pumps it out under through the aorta to the body.

Recent years, many researchers assess the performance of the LV due to the LV function are used for quantifying how well the LV can pump blood through the body with each heartbeat. LV function is an essential parameter in echocardiography as it can alter in several diseases and correlates with various clinical symptoms.

Moreover, the blood flow system can analyze cardiovascular disease. Accurate measurement of blood flow is essential for understanding local flow dynamics. Blood flow velocity is often represented in cm/s, which is inversely related to the total cross-sectional area of the blood vessel and per cross-section. In a healthy heart, the blood flow has laminar characteristics. Thus the blood flow velocity is slowest at the vessel wall and the fastest in the middle of the vessel. Therefore, blood flow visualization studies provide clues to reveal the physiological and pathophysiological mechanism by which abnormal turbulent flow increases cardiac function.

2.4 Cardiac Cycle

Cardiac activity is governed by an electrical impulse which propagates through cardiac tissue and triggers the different phases of a cardiac cycle. This impulse can be measured with an electrocardiogram (ECG). The ECG is a widespread indicator of the phase of the cardiac cycle. The cardiac cycle includes several

different phases, generalized primarily to ventricular systole: isovolumetric contraction (IVC), ventricular ejection (VE); and ventricular diastole: isovolumetric relaxation (IVR), ventricular filling (VF), and atrial contraction (AC). Diastole is characterized by rapid volume expansion of the LV as blood fills the chamber, with a slight pressure rise as the chamber reaches full expansion. Contrast to systole, the rapid volume contraction of the LV results in a pressure that works to eject blood in the circulatory system [Fig.2.5]. Information about different between systolic and diastolic are shown in Table 2.1.

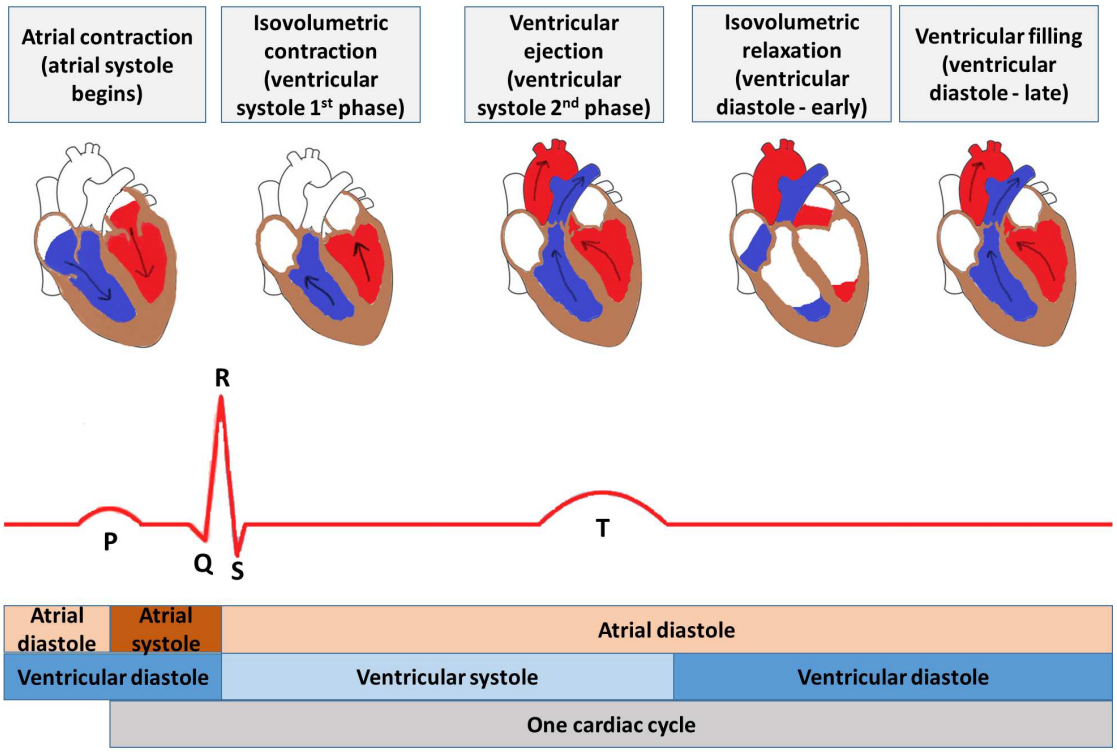

FIGURE 2.5: Cardiac cycle: (top) illustration of blood circulation in heart cavities at each phase, (bottom) diagram depicting cardiac signals (electrocardiogram) of one cardiac cycle.

	Diastolic	Systolic
Definition	It is the pressure that is applied to the walls of the arteries in the body between the heartbeats when it relaxes	it measures the amount of pressure applied to the arteries and blood vessels when the heart beats
Normal Range	60 - 80 mmhg (adult)	90 -120 mmhg(adult)
blood pressure	diastolic represent the minimum pressure in the arteries	systolic represent the maximum pressure exerted on the arteries
Ventricles of the heart	fill with blood	left ventricles contract
blood vessels	Relaxed	contracted
blood pressure reading	the lower number is diastolic pressure	the higher number is systolic pressure

TABLE 2.1: Difference between systole and diastole.

2.5 Aortic Stenosis

Aortic stenosis (AS) is one of the most serious valve disease problems in the developed world [24]. Aortic stenosis restricts the blood to the aorta from the LV due to a narrowing of the aortic valve opening. Thus, LV has to work harder to pump a sufficient amount of blood and onward to the rest of the body. Eventually, the work hard of the heart can weaken the LV, the LV to thicken, enlarge heart overall, and can lead to heart failure problems.

Etiology of aortic stenosis consists of senile calcific degeneration, bicuspid valve, and rheumatic disease. Conventional 2D echocardiography can provide clinically essential information regarding the etiology of the stenosis and the resultant pressure gradient, the valve area, left ventricular function, and hypertrophy. The maximal velocity by the continuous wave Doppler through the aortic valve and pulsed Doppler velocity at the annulus with the continuity equation enable to determine the aortic valve area. As seen in Table 2.2 [25], 2D echocardiography can

provide information regarding the severity of the aortic stenosis, which is essential for the management of patients with aortic stenosis.

Degree	Mean gradient (mmHg)	Aortic valve area (cm^2)
Mild	< 25	> 1.5
Moderate	25 - 40	1.0 - 1.5
Severe	> 40	< 1.0
Very severe	> 70	< 0.6

TABLE 2.2: Severity of aortic stenosis.

In an individual with standard aortic valves, the valve area is 3.0 to 4.0 cm^2 [26]. As aortic stenosis develops, minimal valve gradient is present until the orifice area becomes less than half of ordinary. The pressure gradient across a stenosis valve is directly related to the valve orifice area and the transvalvular flow. As a result, in the presence of a depressed cardiac output, relatively low-pressure gradients can be seen in some patients with severe aortic stenosis. On the other hand, during exercise or other high flow states, systolic impulse-gradients can be measured in patients with minimal stenosis or even standard valves.

2.6 Myocardial Infarction

A myocardial infarction (MI), commonly known as a heart attack, is permanent damage to the heart muscle that occurs when the flow of blood to the heart is blocked. ”Myo” means muscle, ”cardial” refers to the heart, and ”infarction” means the death of tissue due to lack of blood supply.

Your heart is the main organ in the cardiovascular system, which also includes different types of blood vessels. Some of the essential vessels are left ventricular.

The LV obtains oxygenated blood from the LA through the mitral valve and pumps it via the aortic valve into the systemic circulation. When these vessels become blocked or narrowed due to a buildup of plaque, the blood flow in the heart can decrease significantly or stop altogether. Thus This can cause a myocardial infarction.

Numerous studies have evaluated the use of cardiac catheterization in MI, but little is known about the association of LV assessment by either echocardiography or cardiac catheterization with benchmarks of quality care. However, the use of noninvasive diagnostic testing, such as echocardiography in the MI setting has not been well described.

Chapter 3

Two-dimensional Blood Flow Methodology

Medical imaging and medical image computing are seen as a fast-growing field with a fair trend for integrated applications in diagnostics, treatment planning, and treatment [27]. In this chapter, estimating and visualizing two-dimensional (2D) blood flow in the human heart based on CDE has a load of computational algorithms with an understanding of fluid dynamics theories. Some materials in this chapter were published in the ICBIP '18 Proceedings of the 3rd International Conference on Biomedical Signal and Image Processing with title "Correction of Aliasing in Color Doppler Echocardiography Based on Image Processing Technique in Echodynamography" [28] and 2018 International Conference on Orange Technologies (ICOT) with title "Blood Flow Patterns in The Left Ventricle by Echodynamography Method" [29].

3.1 Echocardiography Image Processing

Doppler echocardiography from the ultrasound machine is a digital image. The digital image can be considered as a discrete representation of data possessing both spatial (layout) and intensity (color) information. The digital image is composed of a finite number of elements called pixels, each of which has a particular location and value with intensity $I(m, n)$ where the index m and n determine the location of the rows and columns of the image, respectively.

CDE has true color images where the full spectrum of colors can be represented as a triplet vector, typically red, green, and blue (RGB) components at each pixel location. Color maps provide specific colors for each numeric level in the image to provide a visual representation of the data. CDE has a bit resolution BMP format that can store 24-bit RGB color images.

Because of the original CDE are noisy and unsmoothed, some image processing algorithms are performed on CDE to assess the LV function for eliminating ambiguity in the intrinsic magnitude and direction for Doppler measurements. Image segmentation is commonly used to locate objects and boundaries in images, often based on the characteristics of the pixels in the image. Figure 3.1 (a) show the original image of CDE. Image segmentation is applied to blood flow area as a region of interest (ROI) that is selected biologically motivated. The area of blood flow comes as boundary analysis for a specific purpose.

Image enhancement is the process of improving the quality of CDE image by manipulating the image. Colormaps include any length but must be three columns

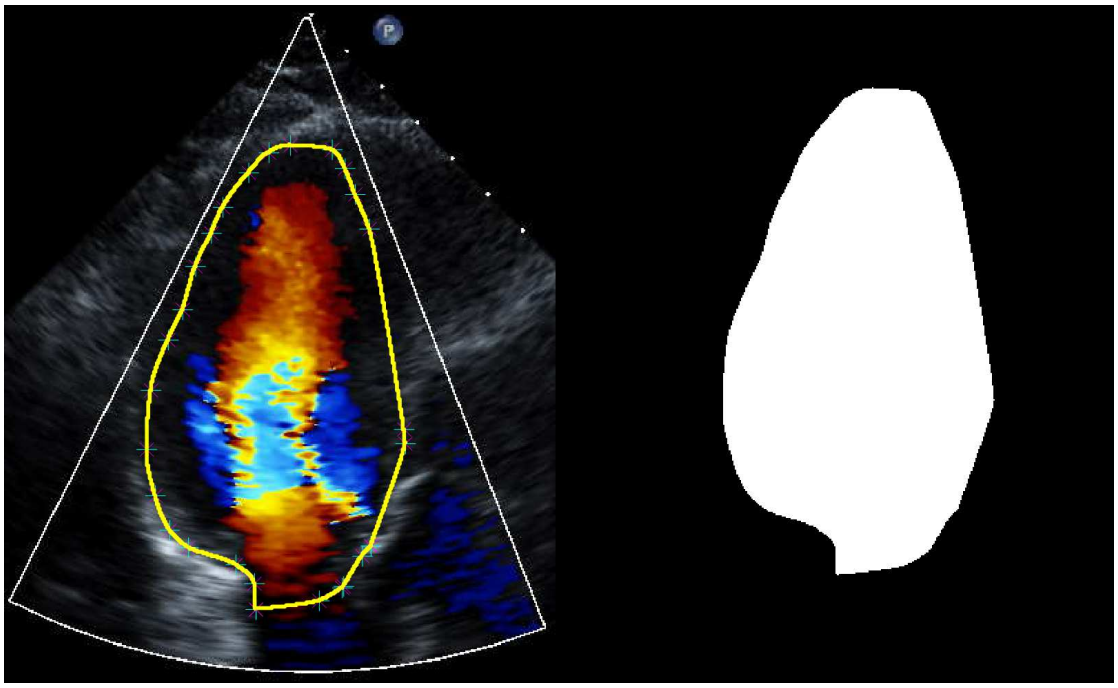

FIGURE 3.1: Image segmentation is applied to blood flow of LV area as a region of interest (ROI) that is selected biologically motivated. The area of blood flow comes as boundary analysis for a specific purpose.

wide which each row in the matrix defines one color using RGB triplets. For example, a pixel whose color components are (0, 0, 0) displays as black, and a pixel whose color components are (255, 255, 255) displays as white. CDE sets colormap to change the visualization color scheme and changing brightness and contrast influence image subjective quality perception [Fig.3.2].

Physiological flow velocities sometimes exceeded low and high Nyquist velocity, resulting in aliasing [Fig.3.1(left)]. Aliasing occurs when the sampled signal is less than twice the highest frequency in the signal. The system does not take enough samples to ascertain which direction the flow occurs. Therefore the scale and direction are displayed incorrectly when the blood flow rate increases and exceeds the Nyquist limit at the half-pulse repetition frequency.

De-aliasing extends the Nyquist velocity range to complete ambiguous estimates

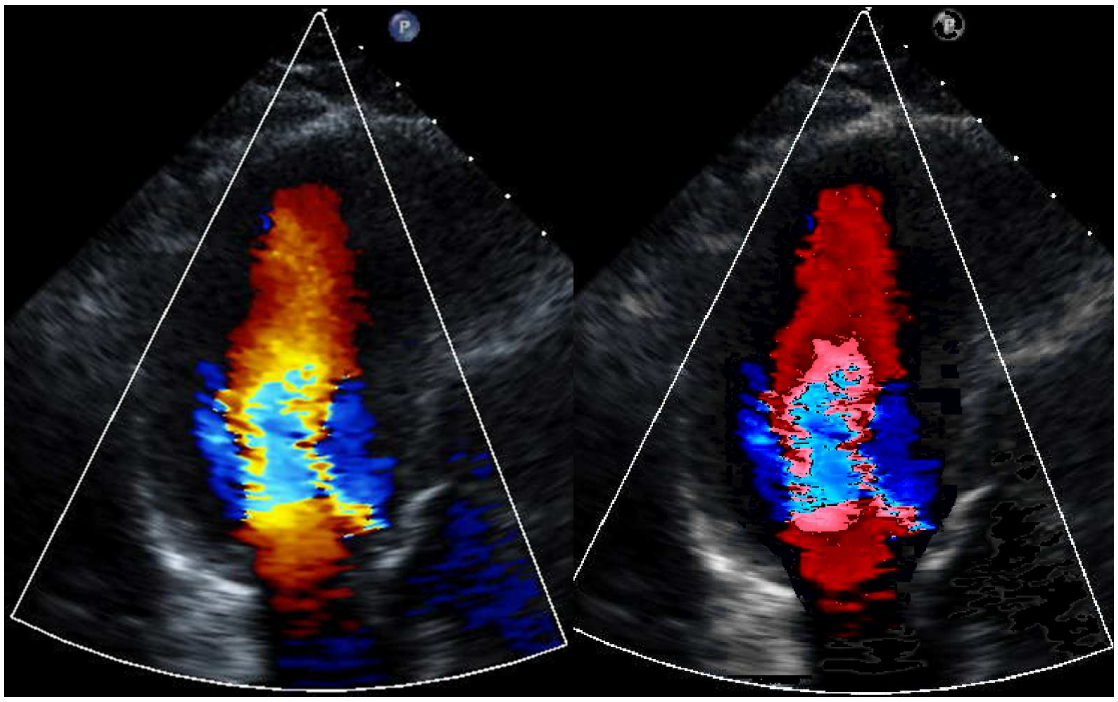

FIGURE 3.2: CDE exceeds low and high Nyquist velocity, resulting in aliasing. CDE sets colormap to change the visualization color scheme and changing brightness and contrast influence image subjective quality perception.

of the direction of blood flow caused by aliasing [Fig.3.3(left)]. An effective speed de-aliasing scheme must be applied to recover the actual signal from the raw measurement. This scheme provides an improvement in speed and direction of actual blood flow, can be expressed as

$$V_t = V_o \pm 2j \times V_{max} \quad k = 0, 1, 2, \tag{3.1}$$

Where V_o is the radial velocity observed, V_t is the velocity of the blood flow that has been changed, V_{max} is the Nyquist velocity interval, and j is the integer multiplier needed to eliminate Nyquist aliasing ambiguity from V_o. The nonzero integer factor j is determined by the difference between the radial velocity measurement and the expected radial speed at the blood data point.

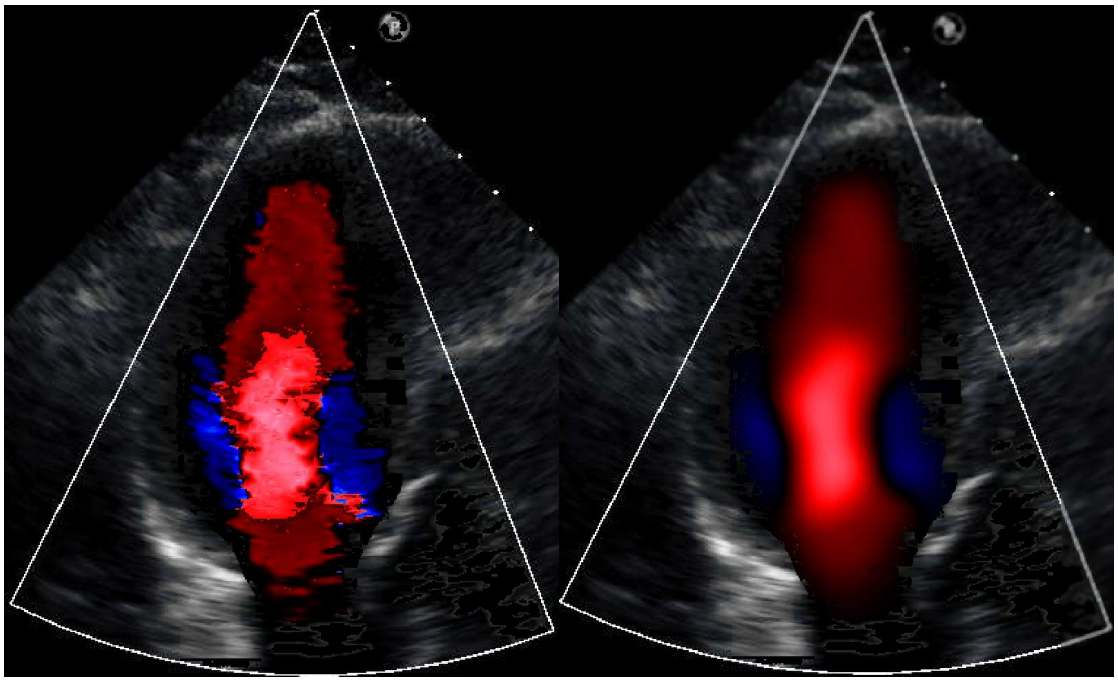

FIGURE 3.3: (left) De-aliasing resolve the ambiguity of the color and direction of blood flow velocity. (right) Median and Gaussian filtering is used to eliminate noise due to the results of the errors in the image acquisition process.

CDE was noisy, requires substantial smoothing to make the representation of the flow plane appropriate. Image filtering is needed to eliminate noise due to the results of errors in the image acquisition process [Fig.3.3(right)].

Smoothing is necessary to stabilize the sufficient data of color Doppler. Both of Median and Gaussian filters are robust concerning missing and additional data. Sufficient data smoothing is necessary to stabilize the differential term. Moreover, velocity smoothing is important. Figure 3.4 show the initial velocity of color Doppler, an effective speed de-aliasing, and velocity smoothing.

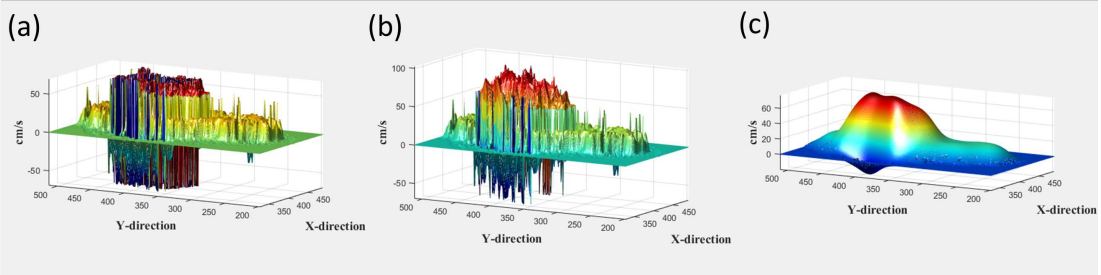

FIGURE 3.4: Plots of the instantaneous flow velocity profile againts positions. (a) original velocity of color Doppler, (b) velocity of color Doppler after applied de-aliasing and (c) velocity smoothing of color Doppler blood flow area of LV in CDE image.

3.2 Echodynamography

Blood dynamics is the study of moving fluids and corresponding phenomena. Fluid in motion has a velocity, just like a solid object in motion has a velocity. The vector velocity is a position function, and if the velocity of the fluid is not constant, then it is also a function of time. Blood flow visualization with spatial and temporal velocity distribution would provide diagnostic and prognostic information on cardiovascular disease.

CDE provides information on one-dimensional (1D) of blood flow far away or approaching the transducer beam [30, 31]. CDE as a tool to obtain intracardiac flow information, consider only details of blood flow velocity far away or approaching the transducer line. Because of these limitations, CDE imaging may not provide adequate information for either the velocity vector distribution and quantitative parameter of hemodynamics.

Echodynamography (EDG) came as an idea of the limited information obtained from CDE. Figure 3.5 represent the radial direction that means the direction of the beam, and the perpendicular direction means the direction of scanning the beam

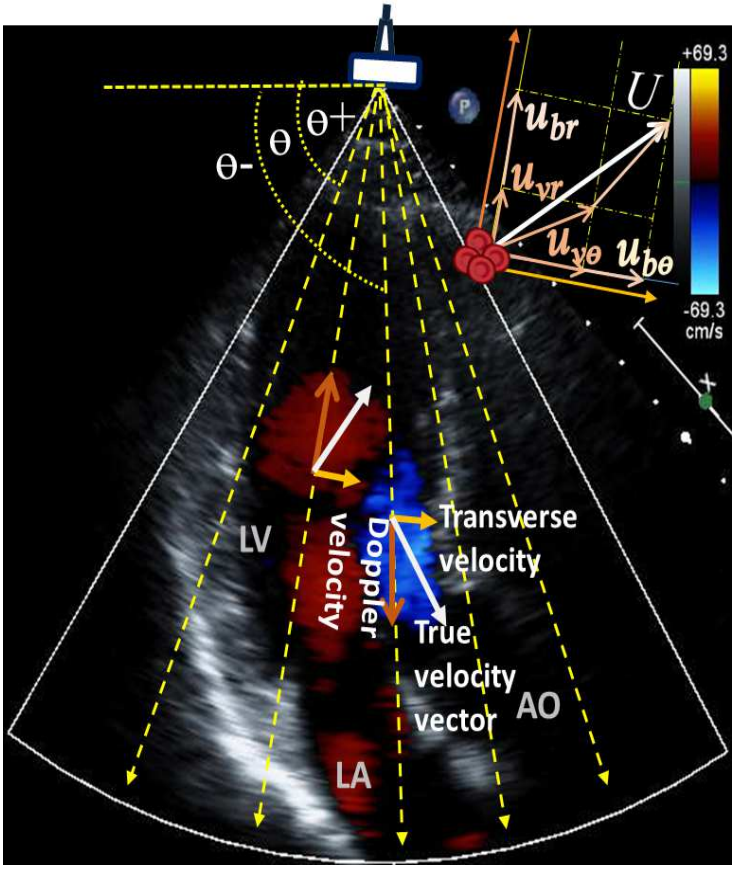

FIGURE 3.5: Apical three-chamber (A3C) view of the EDG method estimates the component of flow velocity in a perpendicular direction. The u_r Doppler velocity at a certain point is the projection velocity along the ultrasound beam. The component of the vortex flow of the longitudinal velocity u_{vr} and the transverse velocity of $u_{v\theta}$ forms the vector of vortex flow component. Likewise, the base flow component of longitudinal velocity u_{br} and transverse velocity $u_{b\theta}$ forms a flow vector of the base flow component. The true flow vector U is calculated by the sum of base u_b and vortex flow u_v components.

from the original line (left side of the sector). Doppler velocity at a certain point is the projection velocity along the transducer beam. The true velocity vector is calculated by the sum of Doppler velocity (longitudinal velocity) and transverse velocity.

EDG is a method of estimating and visualizing three-dimensional (3D) blood flow velocity vectors in two-dimensional (2D) observations plane by applying flow dynamics theory to the Doppler velocity [32, 33]. No boundary conditions were

considered heart-wall flow affected by ventricular wall motion was not included. It helps to better understand the LV hydrodynamics by visualizing the ventricle flow field.

The general form of flow dynamic theory for fluid motion is given by the Navier-Stokes momentum equation [34]:

$$\rho[\frac{\partial \bar{v}}{\partial t} + \bar{v}.\nabla\bar{v}] = \eta\nabla^2\bar{v} - \nabla P + \Delta\rho g\hat{y}, \tag{3.2}$$

where ρ is fluid density, $\frac{\partial \bar{v}}{\partial t}$ is zero for steady-state flows, $\bar{v}.\nabla\bar{v}$ is the inertia term, $\eta\nabla^2\bar{v}$ is diffusion - like the term viscosity, ∇P is the pressure gradient, $\Delta\rho g\hat{y}$ is the buoyancy force, $\bar{v}$ is the fluid velocity. Based on the Navier Stokes equation which describes the movement of a thick liquid substance, the solution is the flow velocity. It is a field since it is defined at every point in a region of space and an interval of time.

In this study, we assume that blood is a Newtonian, incompressible and isothermal fluid, with a constant viscosity of η and a constant density of ρ, there is no forces acting on the bloodstream, there is no source of blood inside an artery [35]. The Navier-Stokes equation satisfy mass conservation which is included implicity through the continuity equation:

$$\nabla.\bar{v} = 0, \tag{3.3}$$

Now consider the irrotational Navier-Stokes equations in particular coordinate systems. In cartesian coordinates with the component of the velocity vector given

by $\bar{v}$ the continuity equation is:

$$\frac{\partial u}{\partial x} + \frac{\partial v}{\partial y} + \frac{\partial w}{\partial z} = 0 \tag{3.4}$$

where the velocity component are defined

$$\bar{v} = (u, v, w) \tag{3.5}$$

the nabla operator is defined as

$$\nabla = (\frac{\partial}{\partial x}, \frac{\partial}{\partial y}, \frac{\partial}{\partial z}) \tag{3.6}$$

The $\bar{v}$ component on the x–y plane is estimated by integrating the continuity equation by assuming the w velocity component in the $z-$direction is ignored $(w = 0)$.

For a 2D incompressible flow, if u_r is a Doppler velocity, which is parallel to the transducer beam namely longitudinal velocity and u_θ is transverse velocity in perpendicular direction. Then $\bar{v}$ components reduces to:

$$\frac{\partial r u_r}{\partial r} + \frac{\partial u_\theta}{r \partial \theta} = 0, \tag{3.7}$$

this leads to the definition of the stream function ψ,

$$\begin{aligned} u_r &= \frac{\partial \psi(r, \theta)}{r \partial \theta}, \\ u_\theta &= -\frac{\partial \psi(r, \theta)}{\partial r}. \end{aligned} \tag{3.8}$$

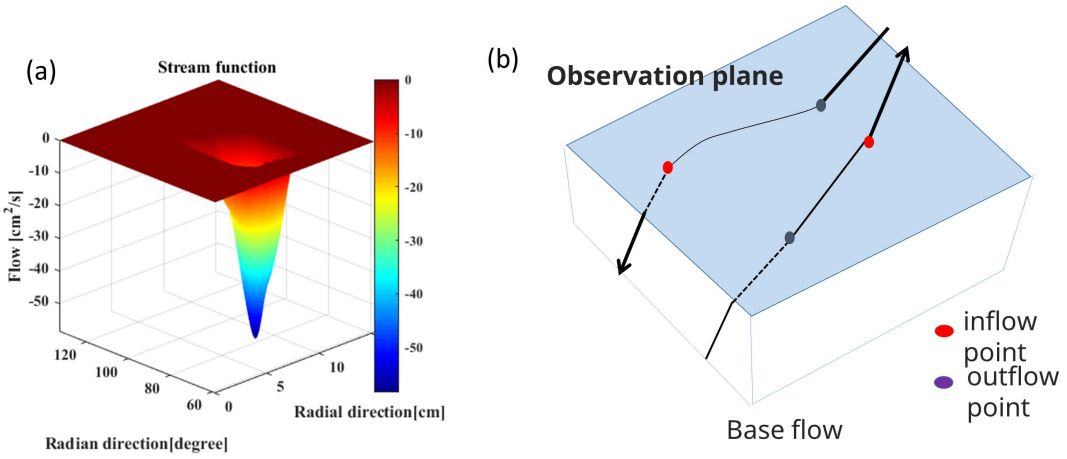

FIGURE 3.6: (a) the z-axis indicates stream function. There is one "cave" corresponding to the one vortex flow. (b) base flow refers to the flow of blood that moves at different points of the straight line parallel to the field of observation.

EDG method divided blood flow into components of the vortex and base flow. The vortex flow refers to the swirling of blood flow that is localized in the field of observation so that the classical "stream function" is applied to obtain the vortex flow vector. Stream function ψ express a flow rate [Fig. 3.6(a)]. Baseflow refers to the flow of blood that moves at different points of the straight line parallel to the field of observation. Propose a new "flow function" to get the base flow vector [Fig. 3.6(b)].

The concept of the EDG method assumes that blood flow is divided into components of the vortex and base flow. Figure 3.7 illustrates the flow rate in the opposite direction from the total flow rate in the observation plane caused the vortex flow (u_{vr}). Otherwise, the flow rate due to being zero or similar direction of the total flow rate causes the base flow (u_{br}).

Here, distance integration of the velocity component u in the beam direction is carried out over distance θ in the direction of r, which intersects perpendicularly

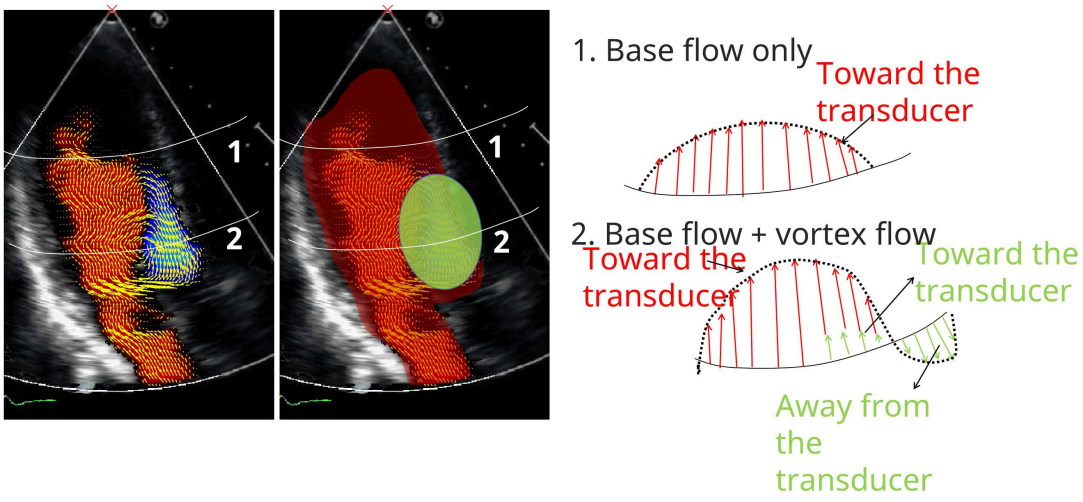

FIGURE 3.7: Example of a 2D blood flow velocity vector produced by EDG. In EDG analysis, CDE images show a combination of base (red) and one vortex (green) flow. Color Doppler data is decomposed into components of the base flow and vortex.

with the beam over the range $[\theta_0, \theta_1]$ of a beam scan, the flux is calculated. Consequently, flux flow $Fc(r)$ is calculated by:

$$F_c(r) = \int_0^{\theta_1} u_r(r, \theta)\ r\ d\theta. \tag{3.9}$$

Figure 3.8 show Doppler velocity in the radial direction is integrated into the perpendicular direction in the irradiation range of the ultrasound beam. Therefore, the EDG utilize this result to estimate transverse velocity.

When calculate this flow distance function, only flux of the positive portion of u is included in F_{c+}, and the negative flux portion is included in F_{c-}, that is

$$F_c(r) = F_{c+} + F_{c-}, \tag{3.10}$$

where the total flow rate is positive, the magnitude of F_{c+} is larger than the magnitude of F_{c-}.

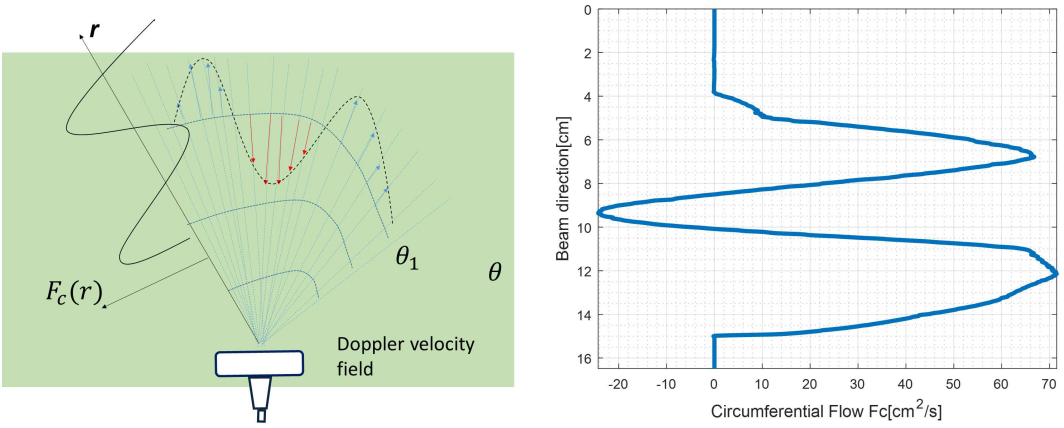

FIGURE 3.8: Distance flow function. Doppler velocity in radial direction is integrated into the perpendicular direction in the irradiation range of the ultrasound beam.

Generally, if the vortex component in a domain is a maximum, the following relation occurs,

$$\psi_+ = -\psi_- = min(F_{c+} + F_{c-}), \tag{3.11}$$

it follows that

$$\psi_- = F_{c-}, \quad \psi_+ = -F_{c-}. \tag{3.12}$$

In this case, k represents the ratio of the positive flux of the vortex to the positive portion of the total flux passing through the integration boundary. Then, the ratio k is defined as

$$k = \frac{\psi_+}{F_{c+}} \begin{cases} only\ vortex\ flow & (k = 1), \\ vortex\ flow\ +\ base\ flow & (0 < k < 1), \\ only\ base\ flow & (k = 0). \end{cases} \tag{3.13}$$

Accordingly, when inflow and outflow in the observation domain occur uniformly,

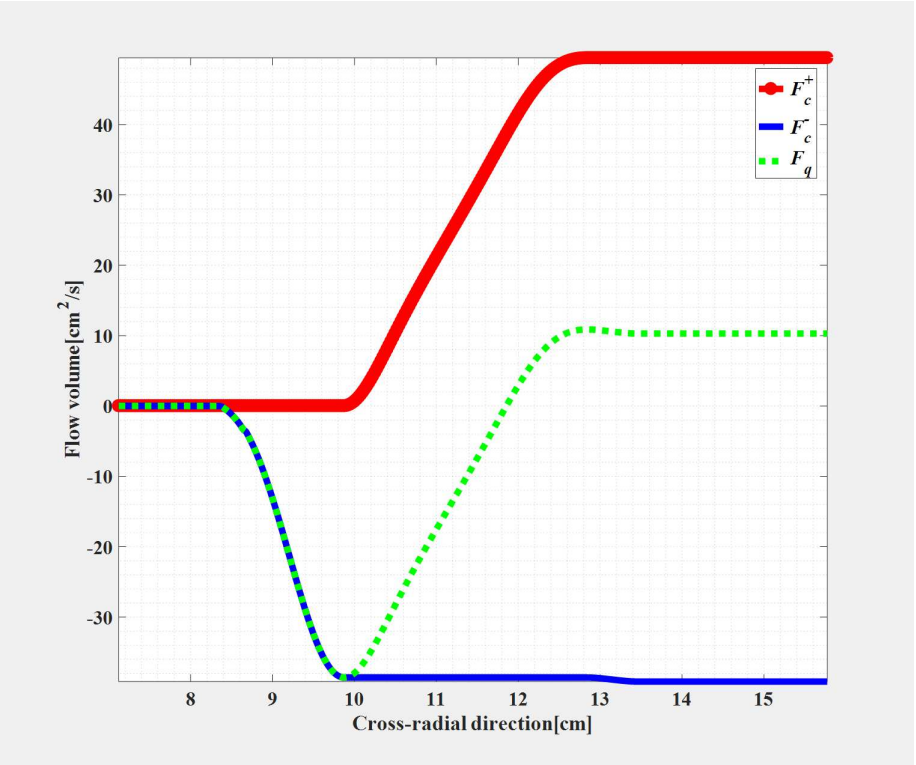

FIGURE 3.9: positive and negative correlation of flow distance function

and the velocity component u is positive, with this assumption, the separation coefficient k $(0 \leq k < 1)$ is determined [Fig.3.10a] as shown in the equation:

$$\begin{aligned} u_{vr} &= k u_r(r,\theta) \quad (u_r > 0), \quad (k = 1) \\ u_{br} &= (1-k) u_r \quad (u_r > 0), \quad (0 \leq k < 0) \\ u_{br} &= 0 \quad (u_r \leq 0). \end{aligned} \tag{3.14}$$

Coefficient $k = 1$ is defined the flow field is vortex flow; coefficient $k = 0$ is defined base flow and $0 < k < 1$ is defined the flow field is a combination of base flow and vortex flow.

Investigation of blood flow to the heart considers sector probe, consider the velocity vector $U = (u_v(r,\theta), u_b(r,\theta))$ in the polar coordinate system as a target [Fig. 3.10b]. A radial direction (r) means the direction of the beam, is a radius ranging

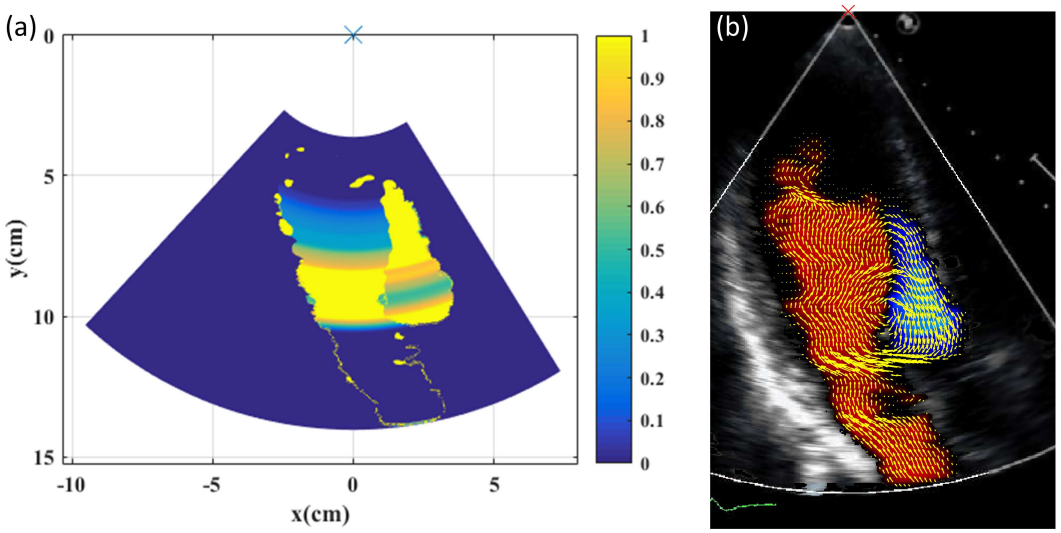

FIGURE 3.10: (a) Separation coefficient of base and vortex flow components. (b) EDG velocity vectors

original to the depth of field. A perpendicular direction (θ) means as the direction of scanning the beam and is an angle ranging from the original line (left side of the sector) to the sector angle.

The longitudinal velocity vector of the vortex and base flow components estimates the transverse velocity vectors in the perpendicular direction. Vortex flow is the flow completed in the observation plane. To determined the vortex velocity in a perpendicular direction ($u_{v\theta}$) can be calculated by stream function, as follows:

$$\psi(r,\theta) = \int_{\theta_i}^{\theta_f} u_r(r,\theta)\ r\ d\theta. \tag{3.15}$$

The θ is the angular coordinates starting from the left side of the transducer [Fig. 3.5]. Then the stream function is calculated in the direction of positive $u^{+}_{v\theta}$ and

the negative direction is $u^{-}_{v\theta}$, as follows:

$$\begin{aligned} u^{+}_{v\theta}(r,\theta) &= -\frac{\partial}{\partial r}\left(\int_{0}^{\theta_f} u_{vr}(r,\theta)\ r\ d\theta\right), \\ u^{-}_{v\theta}(r,\theta) &= -\frac{\partial}{\partial r}\left(\int_{\theta_i}^{0} u_{vr}(r,\theta)\ r\ d\theta\right). \end{aligned} \tag{3.16}$$

Therefore, flow velocity in perpendicular direction of vortex component $u_{v\theta}$ is expressed by the following equation with the weight coefficient of $\xi(0 \leq \xi \leq 1)$, [18]

$$u_{v\theta}(r,\theta) = \xi u^{-}_{v\theta}(r,\theta) + (1-\xi)u^{+}_{v\theta}(r,\theta). \tag{3.17}$$

The base flow component is the flow that includes the flow in and out of the observation plane. Therefore to estimate the continuity equation cannot calculate the base velocity in a perpendicular direction ($u_{b\theta}$). Velocity can be calculated by flow function. the flow function has defined a function and means the base flow rate. The transverse velocity of base flow component in the perpendicular direction can be expressed by the following:

$$\begin{aligned} u_{b\theta}(r,\theta) = -\frac{\partial}{\partial r}\int_{0}^{\theta} u_{b_r}(r,\theta) r\ d\theta \\ + \frac{\partial}{\partial r}\int_{0}^{\theta} (1-k) u_{b_r}(r,\theta) r\ d\theta \\ + (1-k) u_{b_r}(r,\theta)\tan k \end{aligned} \tag{3.18}$$

Thus, the flow velocity in the observation plane of the two velocity components $u_v(r,\theta)$ and $u_b(r,\theta)$ is obtained.

The true velocity vector of blood flow in the EDG method can be written as a sum

of the vortex and baseflow components in longitudinal and transverse velocities, as shown in the equation:

$$U(r,\theta) = u_v(r,\theta) + u_b(r,\theta), \tag{3.19}$$

Figure 3.10(b) shows an example of a 2D blood flow velocity vector generated by the EDG method. In the vector map, the arrow length indicated the magnitude, and inclination of the arrow indicates the direction of blood flow velocities. Therefore, EDG processing visualizes the flow velocity distribution in the magnitude and direction superimposed on CDE image.

Figure 3.11 represent a flowchart of EDG algorithm. EDG method analyzes frame by frame CDE images to visualize 2D velocity vectors using MATLAB R2016b (Mathworks, Natick, MA, WA).

3.3 Hemodynamic Quantitative

We developed a color Doppler echocardiography flow visualization based on fluid dynamics theories, Echodynamography (EDG), which not only shows the intraventricular flow velocity but also estimates vortex, vorticity, and main flow axis line parameters of hemodynamics.

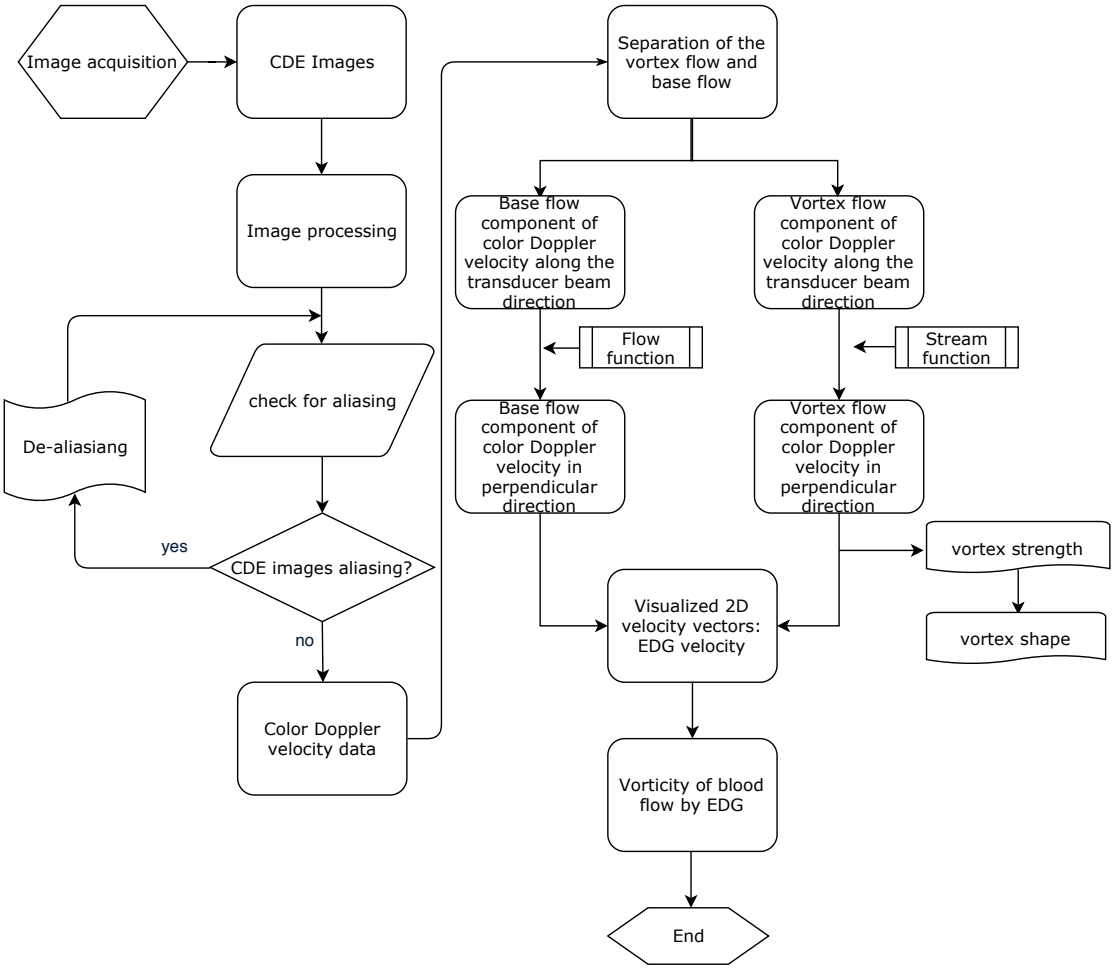

FIGURE 3.11: Flowchart of echodynamography (EDG) algorithm.

Left Ventricle Vortex Flow

EDG is maybe suitable for quantification and assessment of vortex phenomenon in fluid dynamics. The vortex analysis in the LV is a new paradigm for investigating the functional properties of the heart and some risk identifications of cardiac abnormalities [17]. The numerical method of EDG to identify vortex flow in LV has been validated [16]. Several studies used CDE images to investigate the vortex during IVC and VE period [36–40], the vortex flow during a cardiac cycle at the LV in myocardial infarction cases [41] and vortex flow analysis using particle image velocimetry (PIV) [42]. However, these investigations did not provide quantitative

information regarding the vortex in the LV during the cardiac cycle.

Visualizing 2D velocity vectors of blood flow allows further analysis of vortex flow. A vortex is a particular flow arrangement that has a rapid swirling motion around its center. In the present study, the quantitative analysis of the vortex parameters consisted of the vortex strength, vortex shape and Reynolds number as an indicator of the cardiac function [43]. The vortex strength ψ_n (non-dimensionless) described the vortex intensity, using the following equation.

$$\psi_n(r,\theta) = \frac{\psi(r,\theta)}{\Gamma}, \tag{3.20}$$

The parameter Γ is a circulation with a representative length of $L = 0.05$ m, and $U_\propto = 1$ m/s. The blood flow viscosity coefficient is $\nu = 3.454 \times 10^{-6}\ m^2/s$, and the density is $\rho = 1.05 \times 10^3\ kg/m^3$. The parameter Γ can be expressed as follows.

$$\Gamma = \sqrt{U_\propto L \frac{\nu}{\rho}}. \tag{3.21}$$

Figure 3.12 from left to right shows the conventional color Doppler, 2D flow velocity vectors, and contours of the vortex areas. Vortex area contour was measured as the vortex strength. The direction of the vortex is reflected by red (counterclockwise, +) and blue (clockwise, -). For the evaluation of vortex shape, we calculated through the sphericity index ($I_s = \frac{b}{a}$), which defined as the cross-section ratio of the vortex latitude (a) as the horizontal lines and the vortex longitude (b) as the vertical lines. The sphericity index of a circle is one and, by the isoperimetric

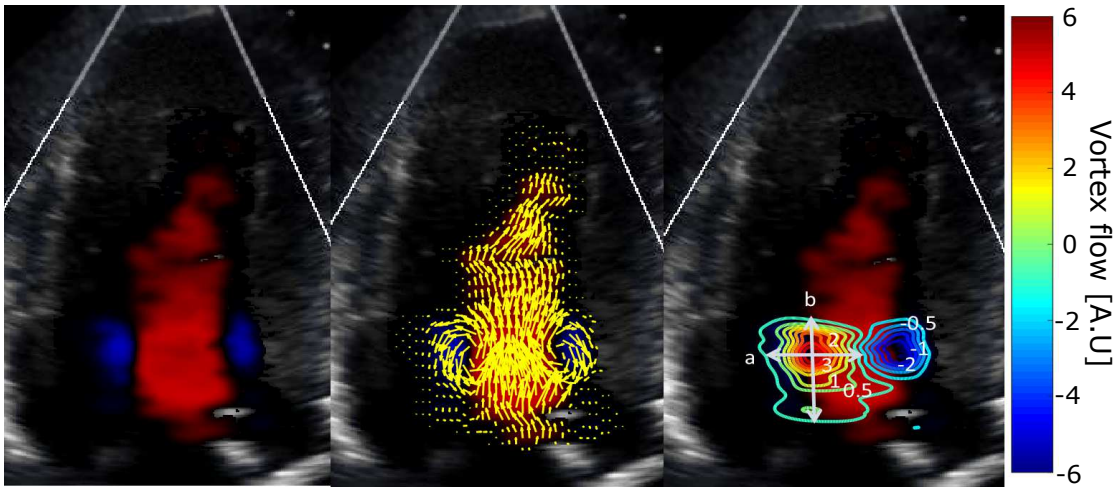

FIGURE 3.12: (Left to right) The conventional color Doppler, Two-dimensional (2D) flow velocity vectors, and the contour of the vortex area. Vortex cavity also describe vortex direction into a region with red (counterclockwise) and blue (clockwise).

inequality, any object which is not a circular will have a sphericity value less than one.

Reynolds number (Re) of vortex depends on the nature phenomena of the vortex shape. The vortex shape form circular or ellipse which is used to calculate the Reynolds number, we calculated the vortex equivalent diameter as follows [44] :

$$de = 1.55\ L^{0.625} /\ P^{0.25} \tag{3.22}$$

$$L = \frac{\pi ab}{4} \tag{3.23}$$

$$P = 2\pi\sqrt{0.5([\frac{a}{2}]^2 + [\frac{b}{2}]^2)} \tag{3.24}$$

The parameter L is the cross-section, P is the ellipse perimeter approximation, and de is vortex equivalent diameter. Re means an important dimensionless quantity in fluid mechanics used to help predict flow patterns in different fluid flow situations,

as follow [45]:

$$Re = \frac{Vde}{\nu}. \tag{3.25}$$

where V was the peak velocity of vortex cavity and ν was the blood kinematic viscosity. Blood viscosity measures the ability of blood to flow through the blood vessels, directly.

Left Ventricle Vorticity

One of important concept in fluid dynamic is vorticity. Vorticity measure of the local rotation of fluid elements and related to the average angular momentum of a fluid particle. Vorticity was calculated from a curl of velocity vectors, transverse velocity in the radial direction should be subtracted with longitudinal velocity in the perpendicular direction, as follow [46]:

$$\begin{aligned} \omega(r,\theta) = \nabla \times \bar{U} &= \frac{\partial r u_\theta(r,\theta)}{r\partial r} - \frac{\partial u_r(r,\theta)}{r\partial\theta}, \\ \omega(x,y) &= \frac{\partial u_y}{\partial x} - \frac{\partial u_x}{\partial y}. \end{aligned} \tag{3.26}$$

Vorticity was associated with the rotational and irrotational flow. Rotational flows were defined as $\nabla \times \bar{U} \neq 0$ at every point in the flow where blood moving, deforming, and rotating. Otherwise, irrotational flows were defined as flows with zero vorticity field, $\omega = 0$ at every point in the flow where blood moving, deforming, and not rotating.

Figure 3.13 displays different colors are filled in vorticity colormap that expressed the rotating direction, and intensity blue represents negative vorticity, a clockwise vortex and red represent positive vorticity, a counterclockwise vortex with brightness represent the intensity of vorticity flow at an arbitrary unit.

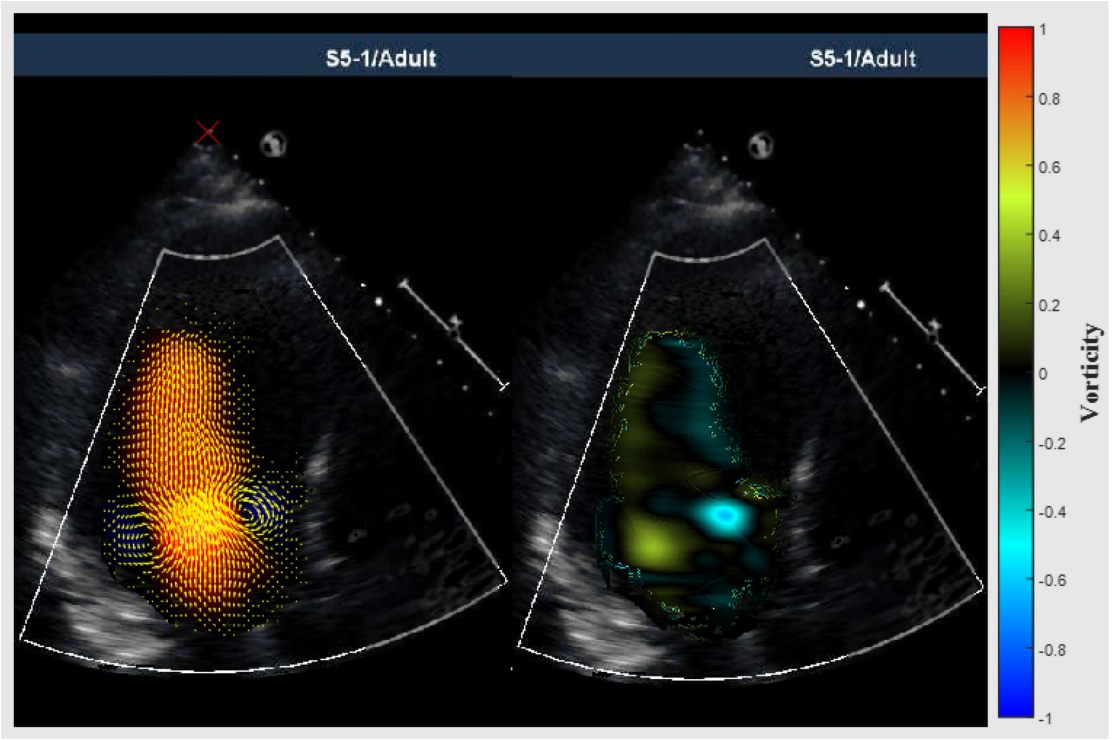

FIGURE 3.13: Vorticity colormap represents the counterclockwise is expressed as positive vorticity, and clockwise is expressed as negative vorticity at an arbitrary unit.

Left Ventricle Main Flow Axis Line

In recent years, the evaluation of LV blood flow has been a significant problem for studying heart function. The main flow axis line has been investigated as a dynamic parameter for assessing heart function in LV ejection [19, 20, 47]. The location and magnitude of maximum velocity occur throughout the blood surface and are related to the structure of intracardiac blood flow and movement of the

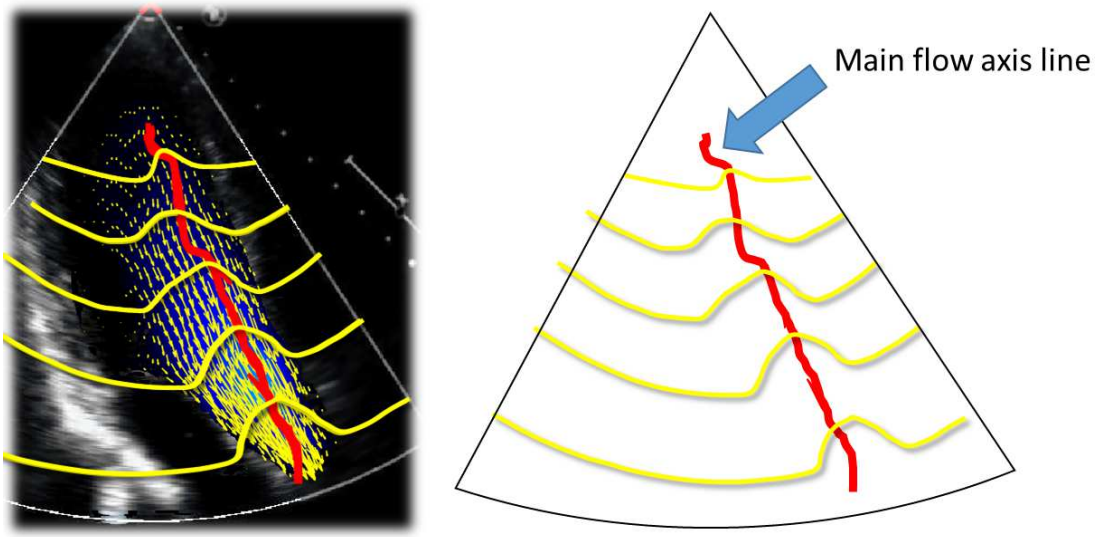

FIGURE 3.14: The red color from apex to LV outflow represents the main flow axis line (MFAL). MFAL is defined as the magnitude of maximum velocity in the perpendicular direction.

heart wall [48] can be considered suitable to represent some typical oceanic physical phenomena [49].

EDG has been proposed as a method of visualizing two-dimensional (2D) blood flow vectors. The vortex energy is related to the vorticity magnitude [36]. However, previous studies have rarely found a vortex during LV ejection and cannot be confirmed by physical theory. Accordingly, this study develops a new method for obtaining the main flow axis line (MFAL) by analyzing the vorticity of the 2D velocity distribution of blood flow so that it became a new assessment to represent heart function in LV.

The MFAL curve gradient measured to analyze the effect of changing the elevation of distance from apex to LV outflow. The MFAL was described as a new assessment for representing a cardiac function in LV. Figure 3.14 illustrates the MFAL with the red line; every point of the red line was a maximum of velocity magnitude in the perpendicular direction. The velocity distribution curve gradient calculates the

adjacent short side ratio (vertical line, y) with the opposite short side (horizontal line, x). A slope angle was an angle that the incline made with the distance of the flow from apex to LV outflow. MFAL is described as a new assessment to represent heart function in LV.

Chapter 4

Particle Image Velocimetry Validation Studies

In this chapter, the basic particle image velocimetry (PIV) including the process of making phantom will be reviewed. Reconstructed velocity of PIV to applied in echodynamography (EDG) method also will be discussed.

4.1 Introduction

EDG is a computational physics algorithm that should be validated when applied to cardiac flow function. The EDG algorithm has been validated by using phase contrast magnetic resonance angiography (PC-MRA) datasets [21, 50]. However, PC-MRA is difficult to implement in routine practice because of limited accessibility and cost. Several medical imaging modalities are used to validate, such as magnetic resonance imaging (MRI) [51–53], computed tomography (CT) [54, 55],

particle imaging velocimetry (PIV) [36, 38, 56]. These instruments have been developed to understand the dynamics of LV flow, which will enable the diagnosis of cardiac abnormalities.

The PIV has become an established measurement technique in fluids mechanics laboratories to measure instantaneous velocity in both research institutes and industry [57]. Therefore, this prospective study was designed to validate the EDG algorithm using virtual color Dopplers of LV phantom obtained by PIV. Thus EDG algorithm has the potential to reveal the pathophysiology of cardiovascular diseases more accurate and reliable.

4.2 In Vitro Experimental Setup

PIV is an experimental study to measure fluid velocity and its related properties. In general, on PIV, liquids are seeded with particles assumed to follow flow dynamics. We created phantom LV, which allows optical observations of blood flow in LV at the same phase and cross section. This innovative *in vitro* system uses the PIV method, which is defined as a flow measurement method that directly determines the velocity field in LV phantom.

An Illustrated experimental component of PIV shown in Fig. 4.1(a). The situation of shooting using a PIV laser (450 mW, Nd: YVO4 at 532 nm, Model: G450 Kato Koken) light source with excellent relative visibility to visualize the field of fluid flow. The fluid flow passing through the LV phantom which was considered to be the bloodstream consists of an aqueous solution of glycerin mixed

polyamide seeding particles (PSP-50, DANTEC Dynamics, density 1.03 g/cm^3, refractive index 1.5) as marker particles. In this study, a final formulation of the PIV fluid when filling the flow phantoms with the fluid, the phantom interface was not visible, confirming that refractive index matched accurately to that of the particular phantom material used [58]. Then, the LV phantom passively pulsated by changing the pressure of the chamber, which was controlled by the commercially available dynamic piston pump (Harvard apparatus pulsatile/ blood pump) at 20 R.P.M rate pump.

An LV phantom was designed using a meshmixer software (x= 45.38 mm, y= 88.80 mm, z= 45.43mm, volume= 10306.8 mm^3) which is not necessarily identical to a physiological condition within a patient. LV phantom was printed using PVA filament on 3D printed molds (TientimeX5 3D printers) at the Saijo Laboratory of Tohoku University. Then, a gel Phantom of LV was employed in the experiment.

The gel phantom of LV was made for PIV measurement from a mixture of dimethyl sulfoxide (DMSO), water and polyvinyl alcohol (PVA) [59]. The procedure followed for the preparation of high tensile strengths, high water contents, and excellent transparency was based on described by [60]. PVA of the same grade described earlier is dissolved in an 8:2 mixture of DMSO and water, to obtain a PVA solution of 15% concentration by weight. Mix DMSO and water, stir for 20 minutes and set rotational speed is 500 rpm, then mix PVA little by little to avoid lumps. The mixture is gently stirred while being maintained at 120^{o}c for 120 minutes. Deaeration allows the air bubbles trapped to migrate to the surface. Then the solution is poured in appropriate containers and refrigerator at -20^{o}c for 24 h.

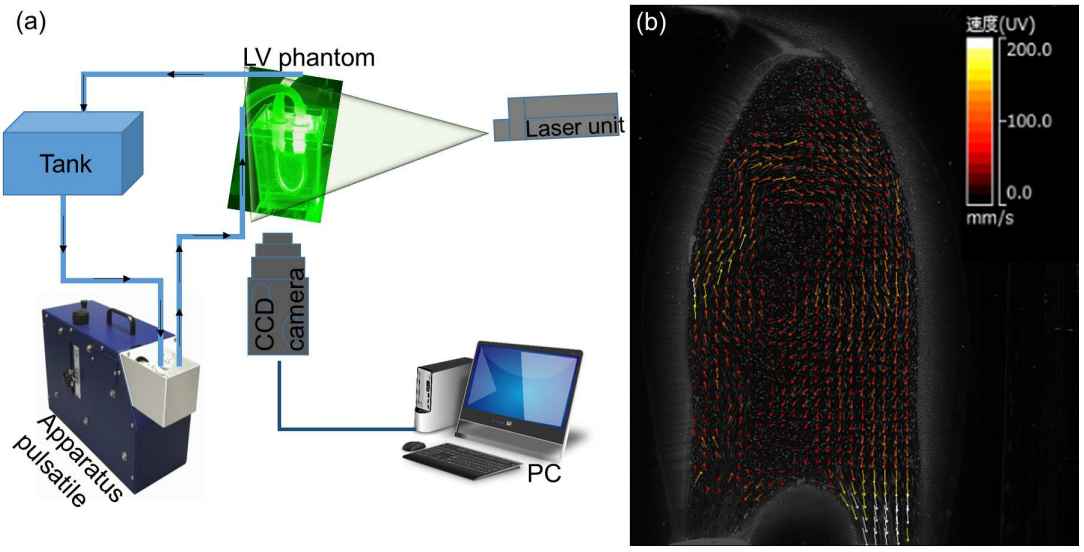

FIGURE 4.1: (a) Illustration of experimental setup for PIV measurements consist of LV phantom, high-speed camera, apparatus pulsatile, laser system, control PC and tank. (b) example of LV phantom flow vectors by PIV measurement.

The resulting LV phantom hydrogels were seen to possess excellent transparency and formed compliant material [61]. Two of nylon pipe connector were attached as the aortic and mitral valve, respectively.

Moreover, the image was captured using a high-speed digital camera (CCD, K-II EX, Kato Koken) at 200 fps (frame per second) to calculate the 2D velocity component by the PIV method. PIV vectors were calculated using high-performance commercial fluid analysis software FlowExpert2D2C. An example of the original LV phantom flow vectors acquired by PIV measurement is shown in Fig. 4.1b.

4.3 Reconstructed Velocity Vectors

The virtual Doppler velocity was defined as the flow components in the direction parallel to the beam direction, directed merely toward or away from virtual sector transducer. The flow pattern was visually assessed by interpreting the field of

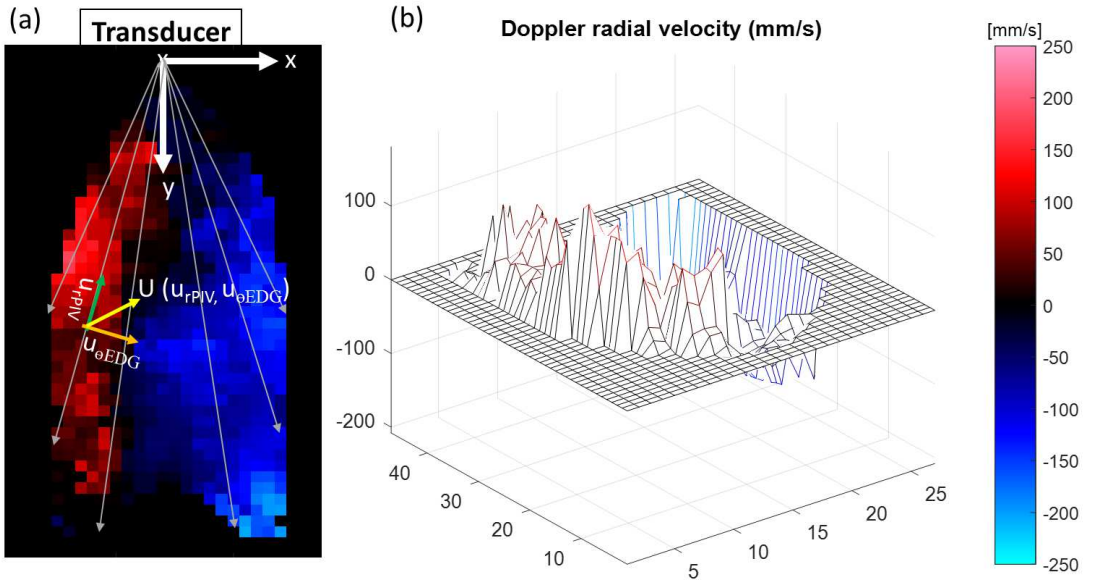

FIGURE 4.2: (a) Illustration of reconstructed velocity vector from PIV to EDG algorithm. (b) A red component shows the flow approaching virtual transducer and blue component show the flow away from the virtual transducer.

longitudinal velocity (u_{rPIV}) using red and blue color-coding. The red color flow indicates the flow toward the transducer and the blue color flow indicates flow mowing away from the transducer, similar to the CDE.

The procedure for validating the EDG algorithm [Fig.4.2(a)], we determined the virtual location of the ultrasound transducer in the cartesian coordinates (x_{vt}, y_{vt}), where x is a horizontal direction, and y is a vertical direction. u_{rPIV} was considered as a virtual Doppler velocity which is defined as longitudinal velocity in the direction parallel to the ultrasound beam, directed to or away from the virtual transducer investigation. u_{rPIV} is applied the EDG algorithm with divided flow velocity into the vortex and base flow to obtain the $u_{\theta EDG}$. Then, We compared the reconstructed velocity field (u_{rPIV}, $u_{\theta EDG}$) and the measured velocity field (u_{rPIV}, $u_{\theta PIV}$) using a linear regression and a Bland-Altman plot.

The point wise error related to numerical reconstruction was defined as the absolute value of the difference between the PIV and the velocity field reconstructed using the EDG algorithm calculated according to the following equations:

$$\epsilon(x, y) = ||U_{PIV} - U_{EDG}||, \tag{4.1}$$

$$E_{tot} = \frac{\int_{LV} \epsilon(x, y) dS}{\int_{LV} ||U_{PIV}|| dS}. \tag{4.2}$$

Where ϵ denotes a pointing error expressed as a function of the Cartesian coordinate (x, y), that is defined as the difference in the absolute value between PIV (original velocity vector measured by PIV, U_{rPIV}) and $U_{\theta EDG}$ (reconstructed velocity vectors obtained by EDG applied on virtual color Doppler). While the norm wise relative error is considered the absolute error divided by the magnitude of the exact value, the percent error is the norm wise relative error expressed in term of per 100.

4.4 Blood Flow Velocity Validation

The EDG method can estimate and visualize two-dimensional blood flow velocity vectors in the human LV [41]. Construct experimental systems validated the EDG method by making the LV cardiac phantom that allows optical and acoustic observations. This experimental system uses the PIV which established as a flow measurement method to measure the velocity field directly within LV. Velocity in the direction parallel to the beam is applied in the EDG method as virtual

Doppler velocity. Then We compare the PIV velocity data with EDG velocity data estimation.

The original of the LV phantom flow vectors by PIV measurements was shown in Fig.4.1b. The image outside of the LV chamber was erased, and the migration of particles in the LV chamber was extracted in the PIV image on the left side. The vectors view on the right side show the flow vectors in the LV chamber based on the PIV image.

Determining the position of the virtual transducer is necessary for comparing the EDG method with the PIV measurement. Similar to color Doppler echocardiography, the position of the transducer is used to obtain a satisfactory beam angle. The cross (x) located at the apex of the LV represents the virtual transducer position. Virtual transducer position is expressed as the red cross in the top of Fig.4.2 showing velocity fields in the direction parallel to the beam measured with PIV. The velocity of PIV is converted into a specific color. The color represents the speed and the direction of flow within a specific area of the image regions (one color pixel). Each of these represents the mean velocity within the region. A red component shows the flow approaching the virtual transducer and blue component flowing away from the virtual transducer. A different shade of red and blue are used to display velocity. In this study, the red mean positive velocity and the blue mean negative velocity.

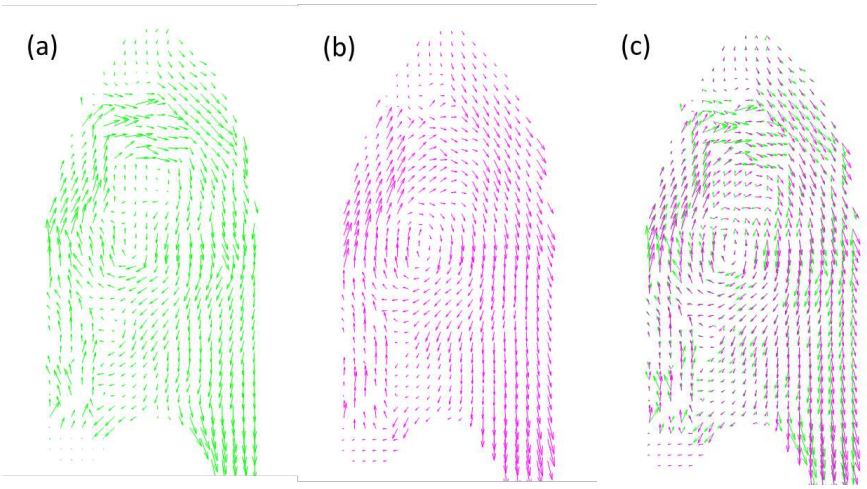

FIGURE 4.3: Two-dimensional velocity vector (mm/s) in the LV phantom showing (a) original PIV measurements (green arrows, u_{rPIV}, $u_{\theta PIV}$), (b) reconstructed velocity vector by EDG method (magenta arrows, u_{rPIV}, $u_{\theta EDG}$) and (b) comparing PIV vs EDG velocity vectors. The image orientation is equivalent to the apical three chamber view.

4.5 Results and Discussion

The velocity field of PIV measured and EDG estimated are shown in Fig.4.3. To quantitatively compare PIV and EDG estimated of two-dimensional velocity field (mm/s) in the LV phantom. Figure 4.3a shows the original PIV measurements (green arrows, u_{rPIV}, $u_{\theta PIV}$), Fig. 4.3b shows reconstructed velocity vector by EDG method (magenta arrows, u_{rPIV}, $u_{\theta EDG}$) and Fig. 4.3c shows comparing PIV vs EDG velocity vectors. Both color and arrow-length encode velocity magnitude. Despite the difference in velocity accuracy between the two methods, the physical features of intraventricular flow such as vortex could be outlined.

Fig.4.4 illustrate the estimated velocity in different time instant during the observed cycle. The red cross represents the virtual transducer position. The flow moves up from a mitral valve at the bottom left to the apex of LV and then flow exit from the aortic valves at the bottom right of each velocity vectors. Similar

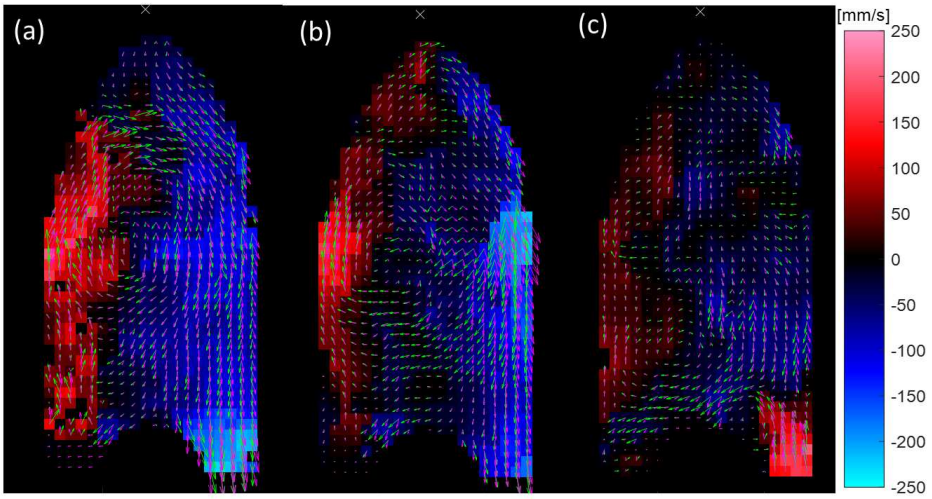

FIGURE 4.4: Two-dimensional velocity vector (mm/s) the *in vitro* experiment of LV phantom showing original PIV measurements (green arrows, u_{rPIV}, $u_{\theta PIV}$) versus EDG method (magenta arrows, u_{rPIV}, $u_{\theta EDG}$). Both color and arrow-length encode velocity magnitude as coded in color bars. Image a, b, and c show a different time instant during the observed cycle. The white cross represents the virtual transducer position.

patterns were observed both in the PIV and EDG results. The physical features such as swirling motion forms moving toward the center of the LV phantom.

Approaching of statistical approved validation of EDG method that accuracy and reliable were analyzed. The correlation between the vectors of the EDG and PIV data at the same point is shown in Fig.4.5. Components of perpendicular direction and radial direction are plotted separately. Each graph using the black lines were obtained using an approximately linear function and R^2 is the determination coefficient. High values of R suggest overall high levels of correlation between all vectors of EDG and PIV data.

Figure 4.5b show the regression analysis for the velocity estimated in the radial direction revealed an excellent correlation ($R^2 = 0.99$, slope $= 0.96$) and Fig. 4.5a moderate correlation in the perpendicular direction ($R^2 = 0.44$, slope $= 0.46$). As revealed by the Bland-Altman plot [Fig. 4.5, Right], however, overestimations and

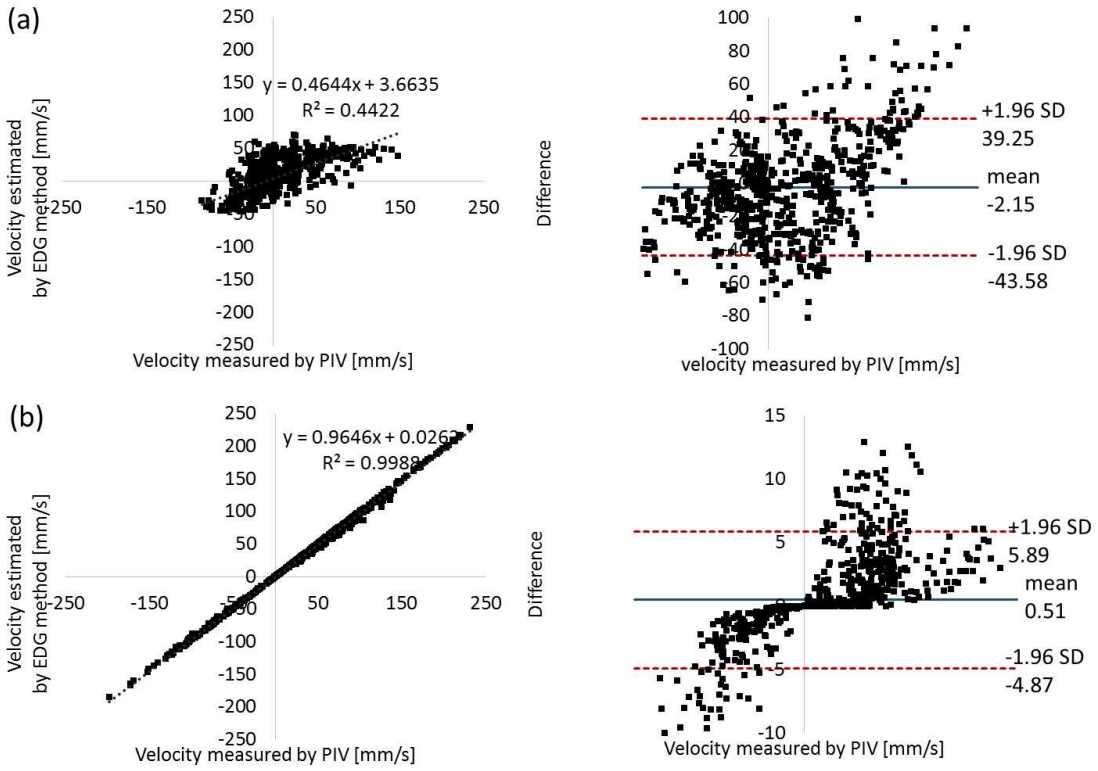

FIGURE 4.5: Statistical analysis. (a) Comparison between velocity measured by PIV and velocity estimated by the EDG method in perpendicular direction. (b) Comparison between velocity measured by PIV and velocity estimated by the EDG method in the radial direction. Different velocity was simulated. SD = standard deviation. The black lines are approximations. R^2 is the coefficient of determination. Correlation depicted as a dotted line, respectively, in the left panel. In the right panel, a solid line indicates mean, and dotted line, SD limits.

higher relative error were observed in the perpendicular direction (0.51 ± 2.75) and in the radial direction (-2.15 ± 21.13), respectively. These findings indicate that good estimates of velocity can be obtained by the EDG method.

Comparison of maximum speed between PIV and EDG in Fig.4.6(a) during the observed cycle using 100 frames during observed cycle. Velocity magnitude showed that the PIV and EDG velocity time histories (frame) closely followed the same trends and are of comparable magnitude. However, the overall velocity magnitude detected by EDG was lower than that detected by PIV. These results indicated that the variance of the velocity was influenced by the error of transverse velocity

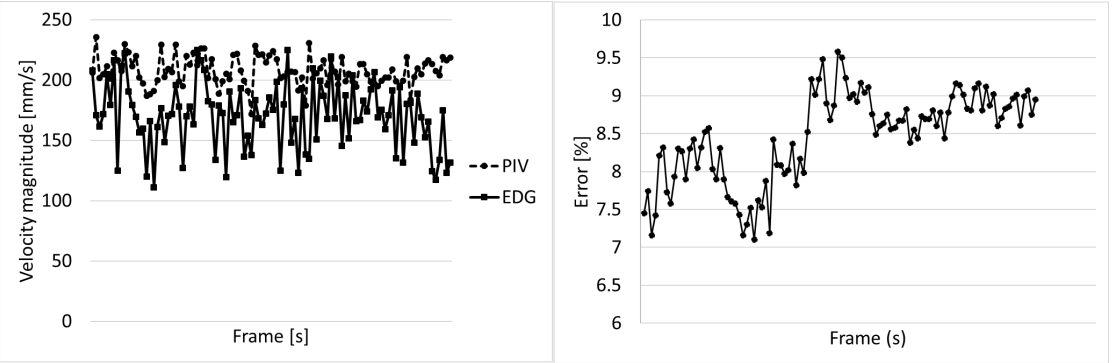

FIGURE 4.6: Statistical analysis: Using 100 frames during an observed cycle concerning the LV phantom data (a) comparison of maximum velocity magnitude between PIV and EDG, (b) relative error of vector discrepancy over EDG and PIV velocity range.

components and may be underestimating the location of the virtual transducer position of the EDG method.

comparison relative error of the vector discrepancy over EDG and PIV velocity range in Fig.4.6(b) during the observed cycle using 100 frames during observed cycle. The relative error results were less than 10%, and the flow pattern was not significantly different from the PIV in the visual observation. However, the flow dynamic of EDG appears to be identical to the PIV measurement both in estimation and visualized blood flow velocity vectors. The statistical distribution of the differences between the velocity magnitudes by PIV and EDG [Fig.4.6] indicates that the velocity vectors obtained by EDG were unbiased and consistent with those obtained by PIV either in terms of relative values or in term of maximum velocity.

Accordingly, EDG provides fairly accurate flow estimation in the LV phantom study. The higher error potentially occurs in cases of LV that have more complex flow. However, the *in vitro* experiment has limitation including the dynamic piston

pump works at a low pumping rate hence provides a low pressure on the LV chamber. While applying high pump rate needs the tensile strength test the LV phantom hydrogel compliancy.

The aim of this study was to assess the validity of EDG for quantitative assessment of the intraventricular blood flow distribution. Accurate mapping of the flow velocity provide novel opportunities to evaluate EDG in *in vivo* estimation. In a basic experimental study using optical PIV, [62] compared phantom chamber flow obtained with anatomical and anti-anatomical positions of mechanical valve and [63] demonstrated LV vortex flow pattern after the mitral surgery using echo-PIV. The similarity of the two studies ensures that these results are the actual vortex patterns inside the cardiac chamber.

4.6 Conclusions

There were several limitations to our study. First, the phantom study was placed on the same plane between the mitral valve and aortic valve directly facing the apex of the LV. Nonetheless, the phantom simulated the nature of the flow reasonably well. Second, there should be a study of repetition of different virtual transducer positions.

This study was validated with a comparative analysis of estimating and visualizing of flow velocity vectors between EDG and PIV data in LV phantom. The experimental study was used to verify the EDG algorithm during the observed cycle. The EDG data agreed well with the PIV measurements in all phases of the

observed cycle. However, in terms of accurately analyzing flow patterns, a small difference is critical. The average relative error of the velocity discrepancy was less than 10%, and the flow pattern was not significantly different from the PIV in the visual observation. Accordingly, EDG is appropriate for estimating and visualizing blood flow velocity vectors in the clinical studies since higher measurement accuracy.

Future study is recommended to compare results with medical imaging modalities which were not included in this study.

Chapter 5

Application for the Clinical Cardiography

In this chapter, the assessment of hemodynamic condition such as blood flow distribution, vortex, vorticity and main flow axis line provide information related to the left ventricular function will be explained. Some materials in this chapter were published in the proceedings of meetings on acoustics with title "Evaluation of blood flow dynamics in healthy and myocardial infarction hearts using Echo-dynamography" [41] and the 2018 40th Annual International Conference of the IEEE Engineering in Medicine and Biology Society (EMBC) with title "Left Ventricular Blood Flow Dynamics In Aortic Stenosis Before And After Aortic Valve Replacement" [64] and also some materials in this chapter were presented in the 41st International Engineering in Medicine and Biology Conference (EMBC 2019) and will be published on international conference proceedings.

5.1 Study Population

Blood flow distribution is closely linked to physiology and pathology of a cardiovascular system [65]. Blood contains oxygen-rich enter the LV chamber from the LA and out the body's tissue through an aorta in a human heart. In the present study, we evaluate the change of blood flow dynamics of myocardial infarction and aortic stenosis patients that compared with healthy participants.

In this study, a total of 21 participants were prospectively enrolled. Six healthy volunteers, eight patients with aortic stenosis (AS), and seven patients suspected myocardial infarction (MI) underwent CDE using iE33 ultrasound system (Philips Ultrasound, Bothell, WA, USA). The study was approved by the Ethics Committee Review Board of Tohoku Pharmaceutical University Hospital, and written informed consent was obtained from all participants.

5.2 Statistical Analysis

All data were presented as mean ± standard deviation (SD). Pearson correlation (r) method analyzed the relation between two parameters and regression linear was calculated for interpreting the slope. Test of group differences of data was performed using one-way analysis of variance (ANOVA). A value of $p < 0.05$ was considered to prove a significant difference. Microsoft Excel 2016 performed statistical analysis.

5.3 Result and Discussion

5.3.1 Echodynamography

Analysis of blood flow velocity vectors in healthy participants by EDG is shown in Fig. 5.1. The instantaneous velocity flow pattern was analyzed frame by frame using EDG on the heartbeat. The yellow arrow of the vector shows the velocity direction, and the yellow length indicates the velocity magnitude by EDG method. The 2D blood flow velocity vectors overlaid on the CDE images. During IVC (11.4 cm/s), VF (73.1 cm/s), and AC (24.9 cm/s) periods, the direction of the vector flow velocity was from LV basal to LV apex with a brief appearance of the vortex at VF and AC. In VE (102.7 cm/s) period, the direction of flow reserved from LV apex to LV basal with a brief appearance of the vortex in the LV outflow tract, well-defined counter clockwise rotational flow. The presence of vortex is common in the cardiovascular system because, when the two atrial chambers contract, additional blood flow is forced into the ventricle.

Figure 5.2 shows the flow velocity vectors in patients with AS during cardiac cycle as examples of the abnormal cases. The blood flow velocity magnitude of exampled AS patients were during IVC (20 cm/s), VE (46.6 cm/s), VF (21.9 cm/s) and AC (47.9 cm/s). The results showed the vortex which was located at the center of the LV during AC and IVC. The vortex flow did not redirect flow coherent as in healthy subject. AS is a disease that affects the pressure in the LA because the aortic valve opening is narrowed, which restricts the blood flow in the LV to the aorta. Therefore, a vortex was nearly generated during the cardiac cycle.

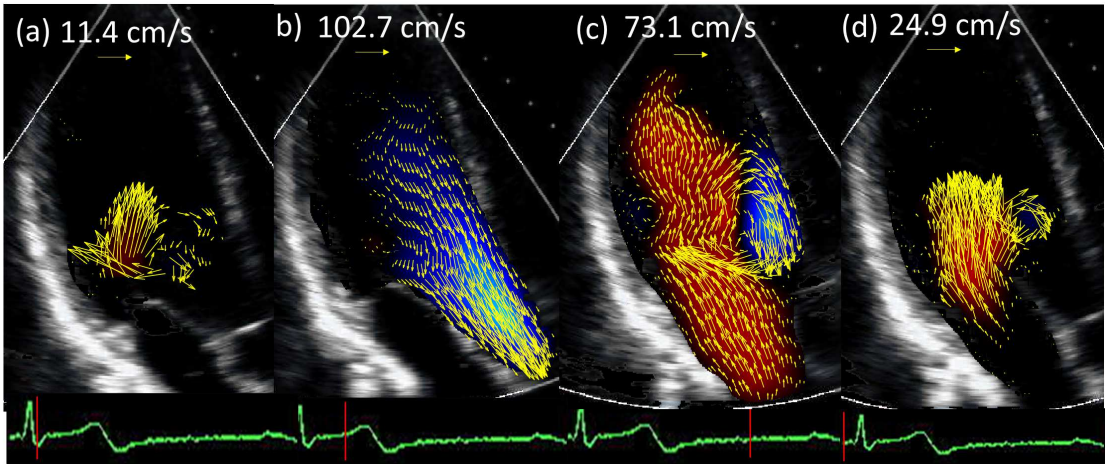

FIGURE 5.1: 2D blood flow velocity vectors visualization overlaid on the CDE images in the healthy LV participants. During (a) isovolumetric contraction (IVC), (b) ventricular ejection (VE), (c) ventricular filling (VF), (d) atrial contraction (AC).

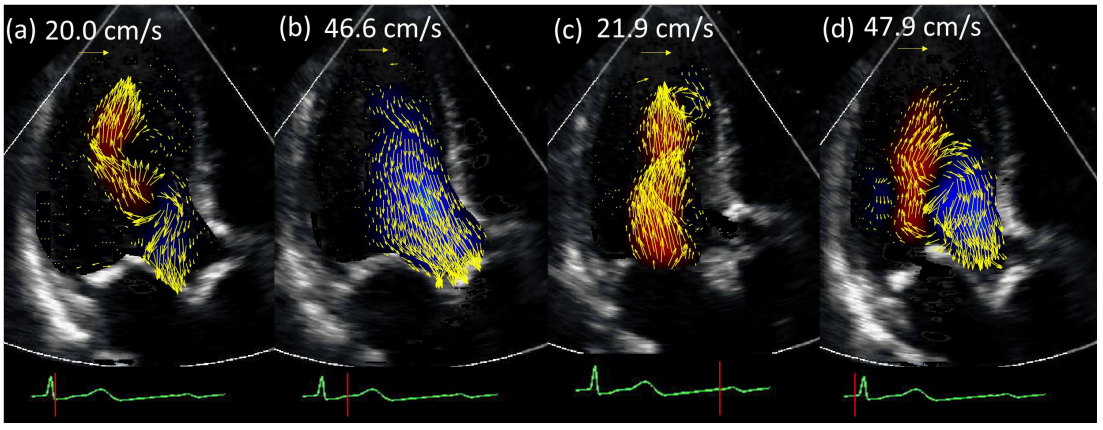

FIGURE 5.2: 2D blood flow velocity vectors visualization overlaid on the CDE images in the abnormal LV of aortic stenosis (AS) patients. During (a) isovolumetric contraction (IVC), (b) ventricular ejection (VE), (c) ventricular filling (VF), (d) atrial contraction (AC).

Figure 5.3 show 2D blood flow velocity vectors visualization overlaid on the CDE images in patients suspected MI during IVC (25.7 cm/s), VE (80 cm/s), Vf(28.3 cm/s), and AC (50.8 cm/s). The results showed the presence of vortex during AC and IVC before VE period. This findings correspond to the vortex ring as described in the previous study.

Comparison between healthy volunteers, AS patients and MI patients looking for

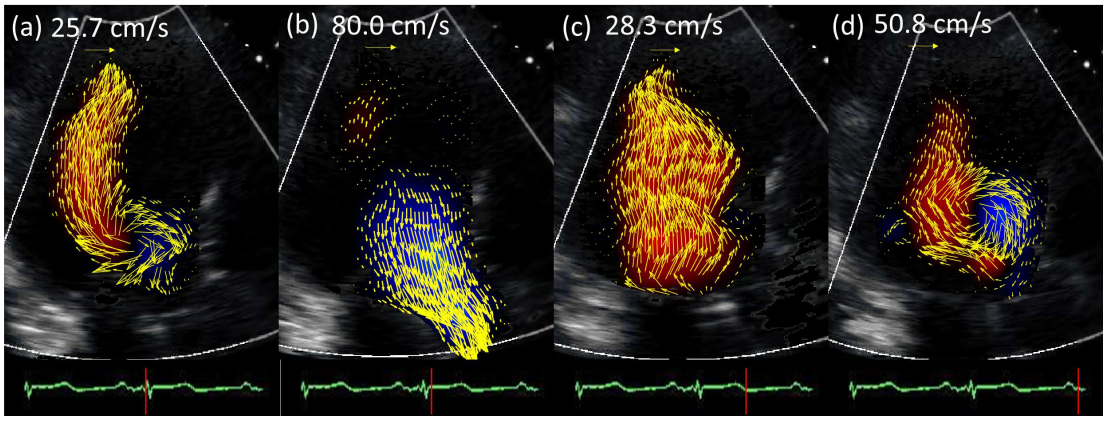

FIGURE 5.3: 2D blood flow velocity vectors visualization overlaid on the CDE images in patients suspected myocardial infarction (MI) during (a) isovolumetric contraction (IVC), (b) ventricular ejection (VE), (c) ventricular filling (VF), (d) atrial contraction (AC).

differences in velocity magnitude showed no significant differences. The highest blood flow during VE period in all participants. Theoretically, blood flowing at higher velocities has a higher ratio of kinetic energy to potential energy.

5.3.2 Vortex Parameters

Figure 5.4 show the vortex strength of LV blood flow visualized with a smooth flow contour. Vortex strength was shown with the codification of a color bar. Red means a positive value that indicates the counterclockwise vortex rotation, and blue means a negative value that indicates the clockwise vortex rotation. The result found the difference of vortex strength during isovolumetric contraction (IVC). The vortex strength in healthy volunteer was -3.5, AS patient was -8 and MI patient was -4.5. Moreover, vortices, a group of blood particles with a swirling motion, of AS and MI patients become complicated and the direction was disordered. It is obvious that the LV systolic dysfunction contributes to signs and symptoms of AS and MI disease.

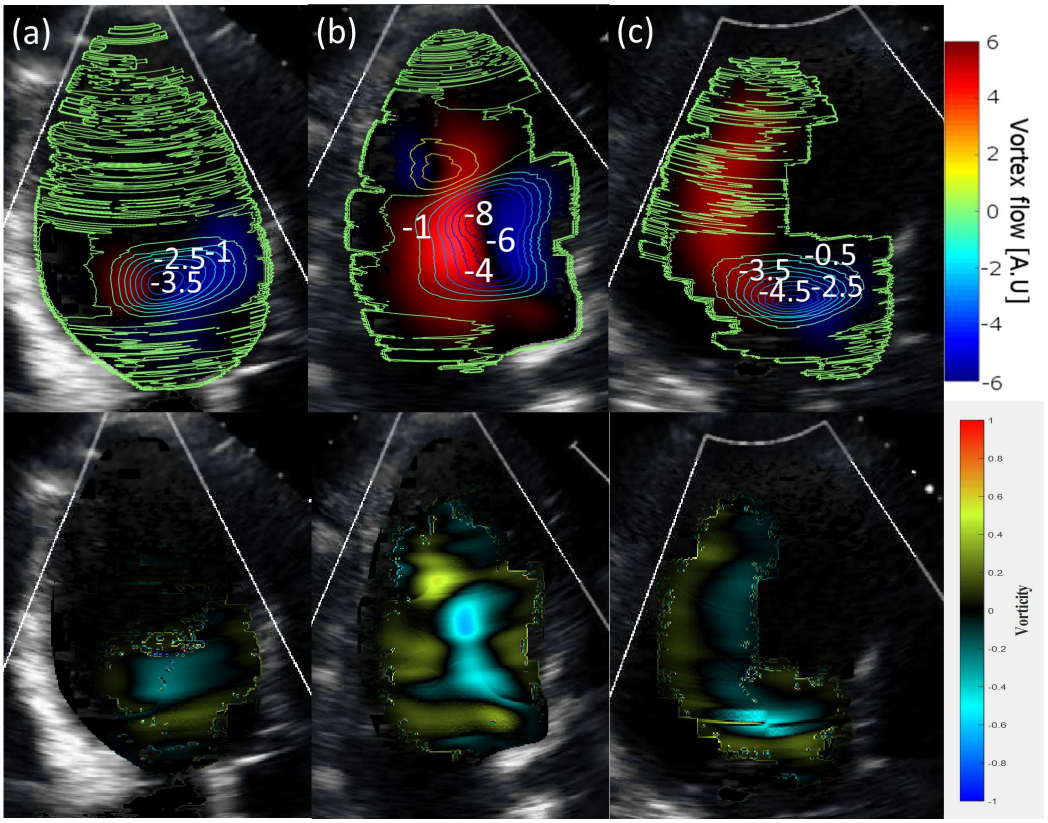

FIGURE 5.4: Contour vortex flow indicated the vortex index of (a) healthy volunteers, (b) AS patients, (c) MI patients during isovolumetric contraction (IVC).

In this study, the clinical investigation of the quantitative parameters of LV vortex flow using EDG method was successfully. The different of vortex parameters between the healthy volunteers, AS patients and MI patients were analyzed as listed in Table 5.1. The results showed that vortex strength (healthy: 3.09±2.06 vs. AS: 5.36±2.81 ($p<0.0001$) vs. MI: 3.32±2.28 ($p=0.184$)) were significantly greatest in the AS patients. The vortex strength indicated the flux intensity of blood flow. The higher the vortex strength, the larger the intensity at the points.

Vortex shape assessment allows understanding LV vortex in flow property changes. For the evaluation of the vortex shape, we calculated the sphericity index (I_s).

TABLE 5.1: Quantitative vortex parameters of healthy, aortic stenosis and myocardial infarction patients.

Vortex parameters	Healthy volunteers (n=6)	Aortic stenosis patients (n=8)	p-value*	Myocardial infarctions patient (n=7)	p-value+
`vortex strength`	3.09 ± 2.06	5.36 ± 2.81	<0.0001	3.32 ± 2.28	<0.184
`Sphericity index`	0.51 ± 0.22	0.99 ± 0.44	<0.0001	0.60 ± 0.27	<0.626
`Reynolds number`	1020 ± 603	2405 ± 1562	<0.0001	1290 ± 913	<0.137

p-value*: between healthy and aortic stenosis.
p-value+: between healthy and myocardial infarction.

The vortex sphericity index (I_s) were significantly higher in AS patients, compared with MI patients and the healthy LV function group (healthy: 0.51±0.22 vs. AS: 0.99±0.44 (p<0.0001) vs. MI: 0.60±0.27 (p=0.626)) . In healthy subjects, the average vortex was compact, elliptically shaped proved with sphericity index (I_s) less than one, and was located apically. In patients with abnormal LV function group, a spherical, centrally located vortex was observed with the incoherent direction of LV flow. The previous study found the similar results in abnormal condition, the vortex possesed a more spherical shape as, confirmed by a reduced I_s [36].

Table 5.1 show Reynolds number (healthy: 1020±603 vs. AS: 2405±1562 (p<0.0001) vs. MI: 1290±913 (p=0.137)) were significantly greater in the AS patients than in MI patients and the healthy volunteers. Through Reynolds number, we determine the type of flow. The turbulent flow occurs during the higher Reynolds number. AS and MI patients was confirmed the higher Reynolds number. The incidence of turbulent flow increases with Reynolds number, which is increased with either the elevation of blood flow velocity. Also, as a vortex enlarge, energy loss occurs worsening cardiac function.

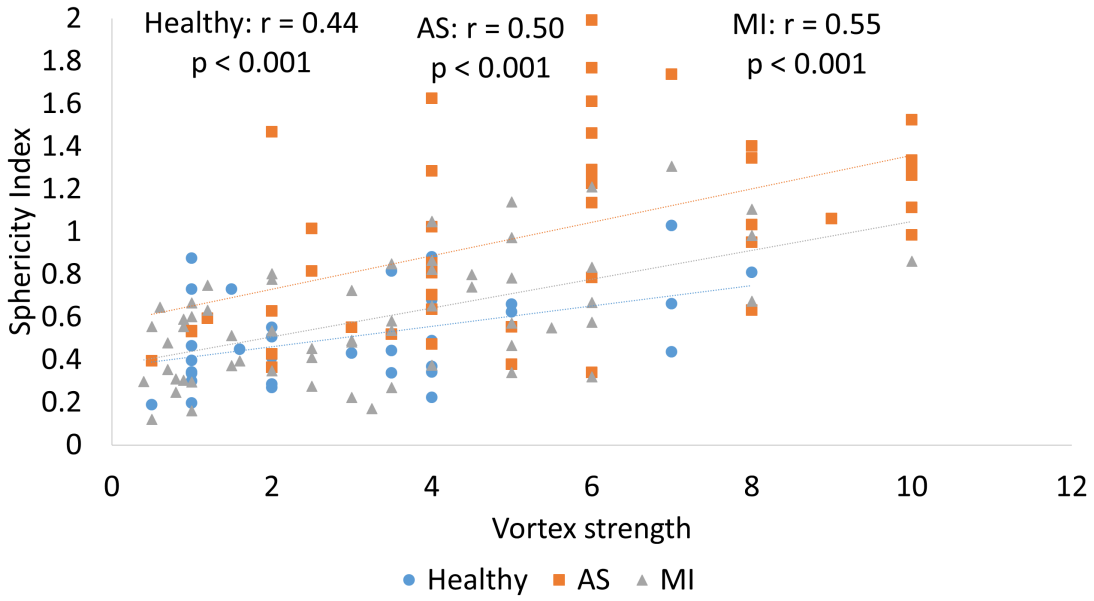

FIGURE 5.5: Scatterplots showing the correlation between sphericity index and vortex strength. Blue circle indicate data from the healthy volunteers, orange square indicate data from AS patients and grey triangle indicate data from MI patients.

Figure 5.5 represents the correlation between sphericity index and vortex strength in all participants. The results showed the vortex sphericity index have a positive correlation with vortex strength in all participants (healthy: r=0.44, $p < 0.001$, AS: r=0.5, $p < 0.001$, MI: r=0.55, $p < 0.001$). However, there is no significant difference of sphericity index and vortex strength if compared in each group participants.

Figure 5.6 represents the correlation between vortex strength and Reynolds number in healthy volunteers (blue, circle), aortic stenosis (AS) patients (orange, square), and myocardial infarction (MI) patients (grey, triangle). The results showed the vortex strength have a positive correlation with Reynolds number in all participants (healthy: r=0.79, $p = 0.29$, AS: r=0.98, $p < 0.001$, MI: r=0.85, $p = 0.033$).

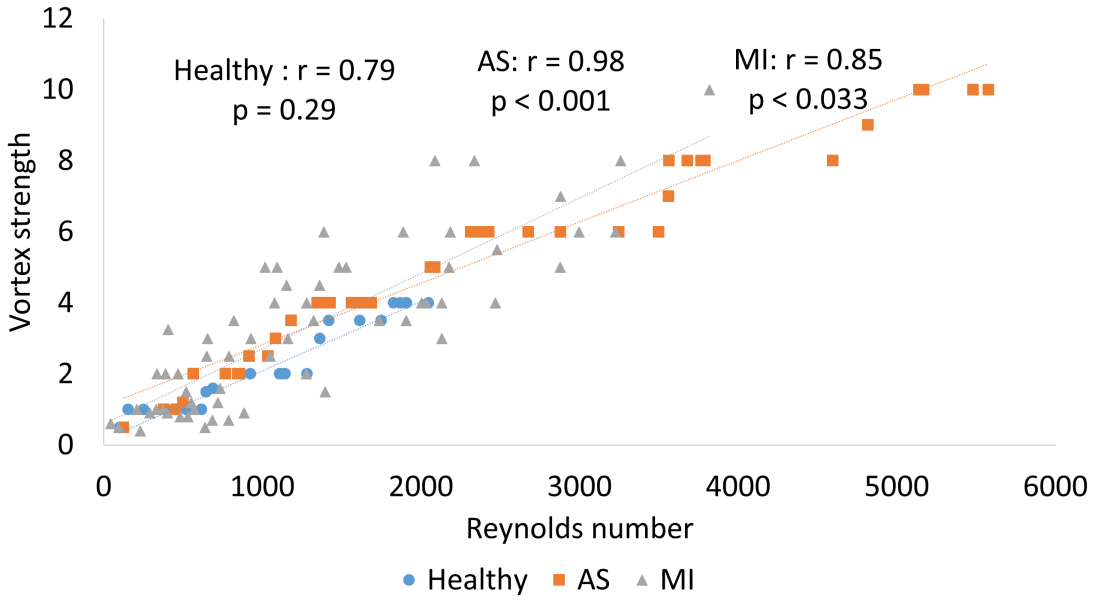

FIGURE 5.6: Scatterplots showing the correlation between vortex strength and Reynolds number in healthy volunteers (blue, circle), aortic stenosis (AS) patients (orange, square), and myocardial infarction (MI) patients (grey, triangle).

Figure 5.6 represents the correlation between vortex sphericity index and Reynolds number in healthy volunteers (blue, circle), aortic stenosis (AS) patients (orange, square), and myocardial infarction (MI) patients (grey, triangle). The results showed the vortex sphericity index have a positive correlation with Reynolds number in all participants (healthy: r=0.21, $p < 0.001$, AS: r=0.47, $p < 0.001$, MI: r=0.47, $p < 0.001$).

Moreover, Reynolds number have tendency to present the larger range in abnormal cases than normal cases. The previous study found the local Reynolds number based on the mean velocity (18 cm/s) at the valve orifice area, was 840, indicating a laminar flow regime across the valve and Reynold number was 5500, indicating the flow was in the laminar-turbulent transitional regime [66]. Several quantitative parameters for describing vortex properties have been reported, including vortex strength, vortex shape (sphericity index), and vortex Reynolds number.

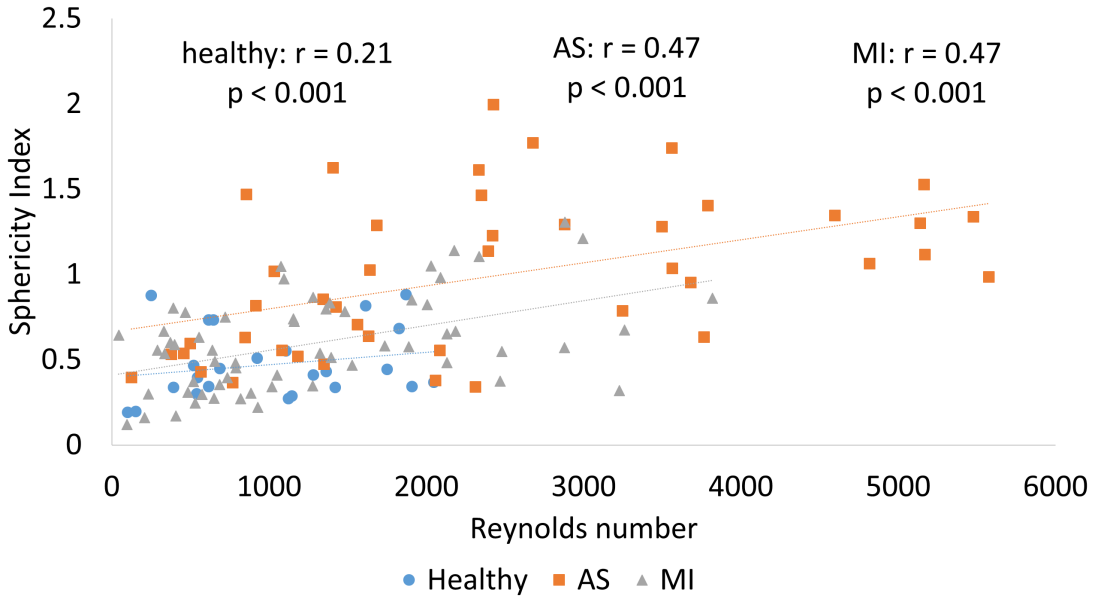

FIGURE 5.7: Scatterplots showing the correlation between vortex sphericity index and Reynolds number in healthy volunteers (blue, circle), aortic stenosis (AS) patients (orange, square), and myocardial infarction (MI) patients (grey, triangle).

Parameters related to the vortex flow would be associated with the prognosis of ventricular performance. In the previous reports, only geometrical features of the vortex that form have been reported.

5.3.3 Vorticity and Main Flow Axis Line

In the present study, 2D vorticity color map of blood flow was presented during VE in LV. Vorticity was represented in degradation color which denoted the blood flow in the clockwise direction as red dark, and blue dark signified the blood flow in the counterclockwise direction. Blood flow produced vortex motion in the clockwise direction, with red sharpness differently. This result may be associated with the difference of blood flux intensity within a local rotation according to the sharpness of the color bar which is expressed by arbitrary unit [A.U] on the right side figure.

This study observed MFAL of healthy participants during ventricular ejection period, especially [Fig. 5.8]. Two-dimensional (2D) of flow velocity vectors, two-dimensional (2D) of vorticity estimation by EDG and one-dimensional (1D) flow axis line superimposed on vorticity images during ventricular ejection in LV and aorta of MI patients was estimated. The velocities of ejected blood flow in the normal heart were in early systole (117.1 cm/s), mid systole (89.1 cm/s), and late systole (49.1 cm/s). Blood flow proceeded form swirling motion during late systole in normal LV. One vortex was generated near the base area of LV that may indicate that LV progress to the diastole phase immediately.

This study observed MFAL of AS patients during ventricular ejection period, especially [Fig. 5.9]. Two-dimensional (2D) of flow velocity vectors, two-dimensional (2D) of vorticity estimation by EDG and one-dimensional (1D) flow axis line superimposed on vorticity images during ventricular ejection in LV and aorta of MI patients was estimated. The velocities of ejected blood flow in the abnormal heart were in early systole (89.1 cm/s), mid systole (98.9 cm/s), and late systole (67.6 cm/s).

This study observed MFAL of MI patients during ventricular ejection period, especially [Fig. 5.10]. Two-dimensional (2D) of flow velocity vectors, two-dimensional (2D) of vorticity estimation by EDG and one-dimensional (1D) flow axis line superimposed on vorticity images during ventricular ejection in LV and aorta of MI patients was estimated. The velocities of ejected blood flow in the MI were in early systole (68.5 cm/s), mid systole (67.4 cm/s), and late systole (48.6 cm/s).

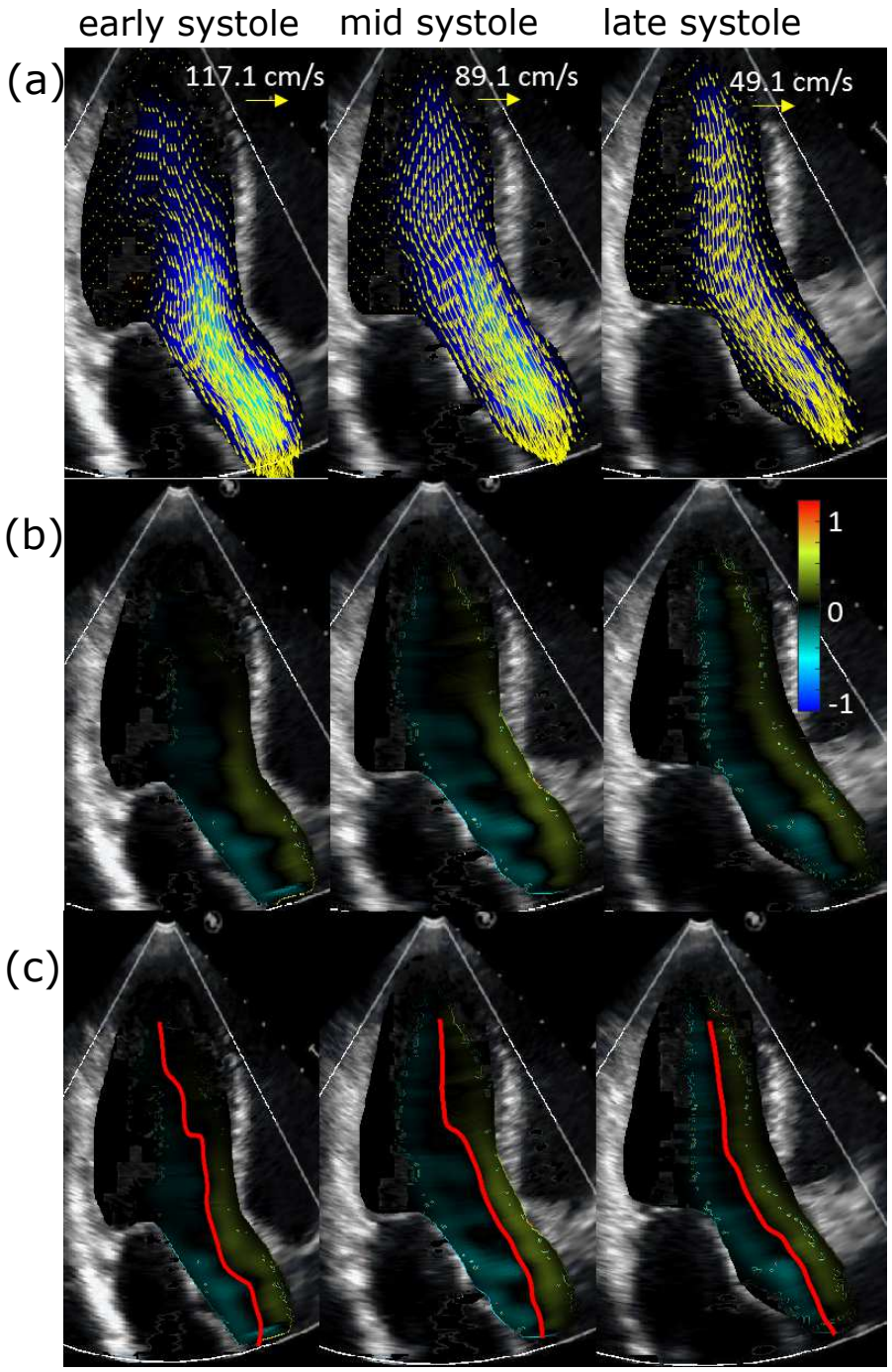

FIGURE 5.8: (a) Two-dimensional (2D) of flow velocity vectors, (b) two-dimensional (2D) of vorticity estimation by EDG and (c) one-dimensional (1D) flow axis line superimposed on vorticity images during ventricular ejection in LV and aorta of healthy volunteers.

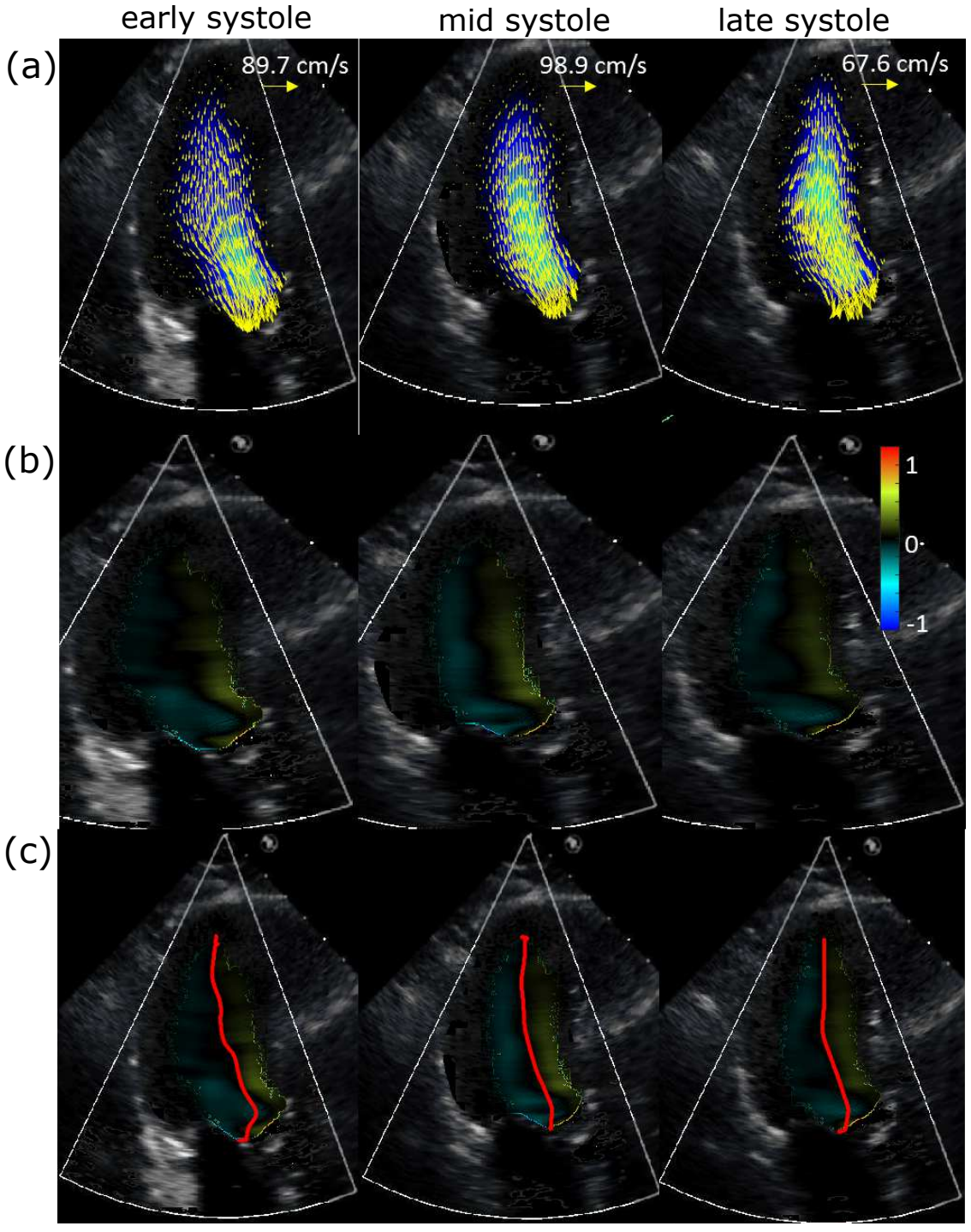

FIGURE 5.9: (a) Two-dimensional (2D) of flow velocity vectors, (b) two-dimensional (2D) of vorticity estimation by EDG and (c) one-dimensional (1D) main flow axis line superimposed on vorticity images during ventricular ejection in LV and aorta of AS patients.

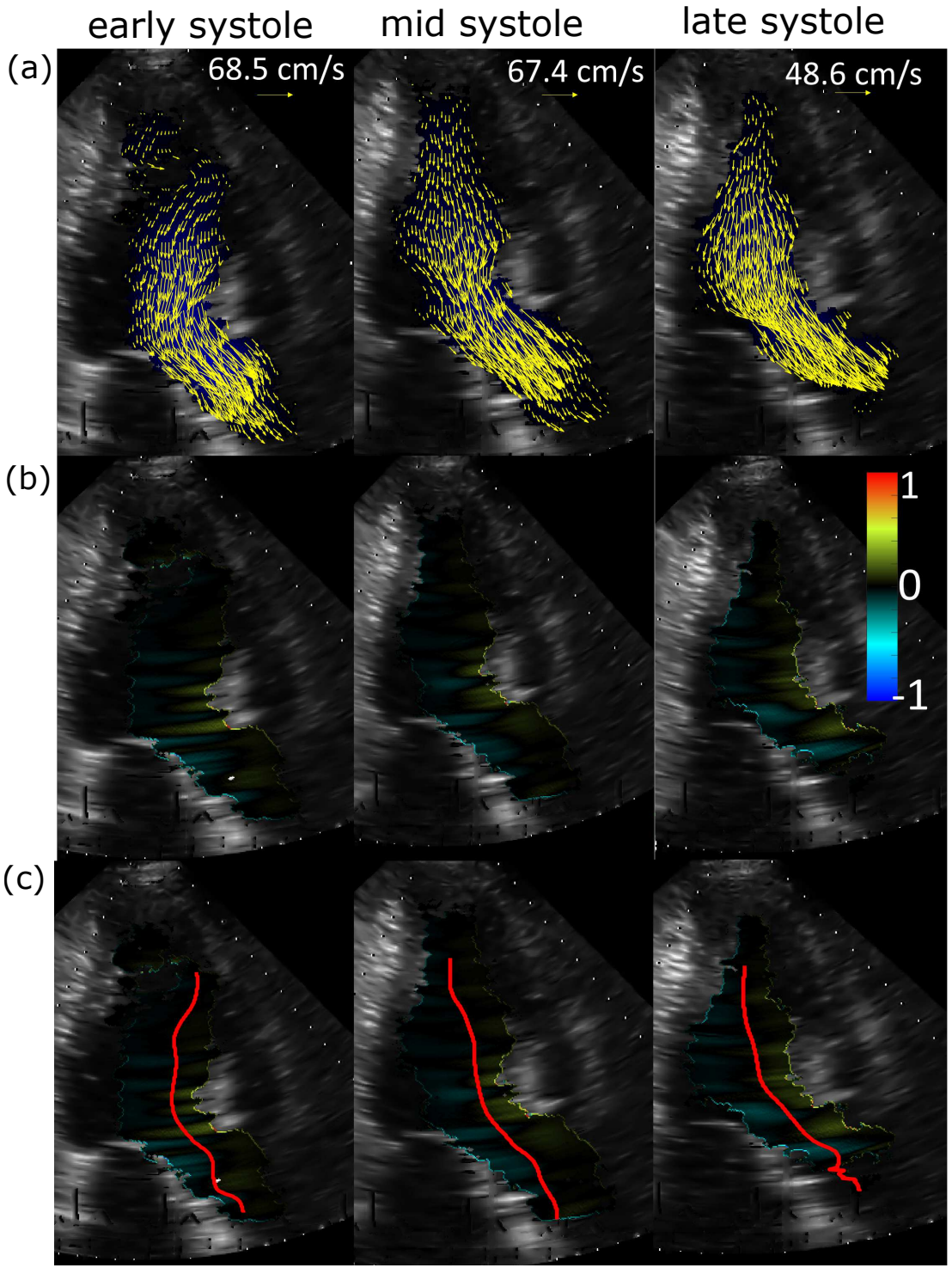

FIGURE 5.10: (a) Two-dimensional (2D) of flow velocity vectors, (b) two-dimensional (2D) of vorticity estimation by EDG and (c) one-dimensional (1D) flow axis line superimposed on vorticity images during ventricular ejection in LV and aorta of MI patients.

MFAL started from apex to LV outflow. The position of maximum velocity in the perpendicular direction established MFAL that through the vorticity path which is zero, $\omega = 0$, that indicated the irrotational flow. MFAL were compared between healthy volunteers, AS patients, and MI patients. The results of MFAL show the dynamics during LV ejection with vortex formed and pressure increased as cardiac muscle contract to hard squeeze LV in the whole direction in AS patients.

Blood flow velocity distribution curve (VDC) on the MFAL was obtained, and the maximum slope of the VDC was measured. Figure 5.11, Fig.5.12, and Fig.5.13 show the blood flow velocity distribution curve (VDC) on the MFAL in healthy volunteers, AS patients, and MI patients during early, mid and late systoles. Figure 5.11 showed a significantly curve increased velocity of blood flow during nearly the LV outflow. VDC started in the apex, gradually increased in the center and steeply increased in the base of LV in the healthy heart.

Figure 5.12 show the blood flow velocity distribution curve (VDC) on the MFAL in AS patients. VDC started in the apex which was downward convex. The flow linearly toward to LV outflow during early systole, increased during mid-systole, and almost linear during late systole. The blood flow velocity curve showed the dynamics of blood flow in LV which related to the effect of narrowing the aortic valve opening of AS patients.

Figure 5.13 show the blood flow velocity distribution curve (VDC) on the MFAL in MI patients. Blood flow was not observed at the apex. The MFAL started from the center of LV, and the flow linearly increased toward to LV outflow in MI patients.

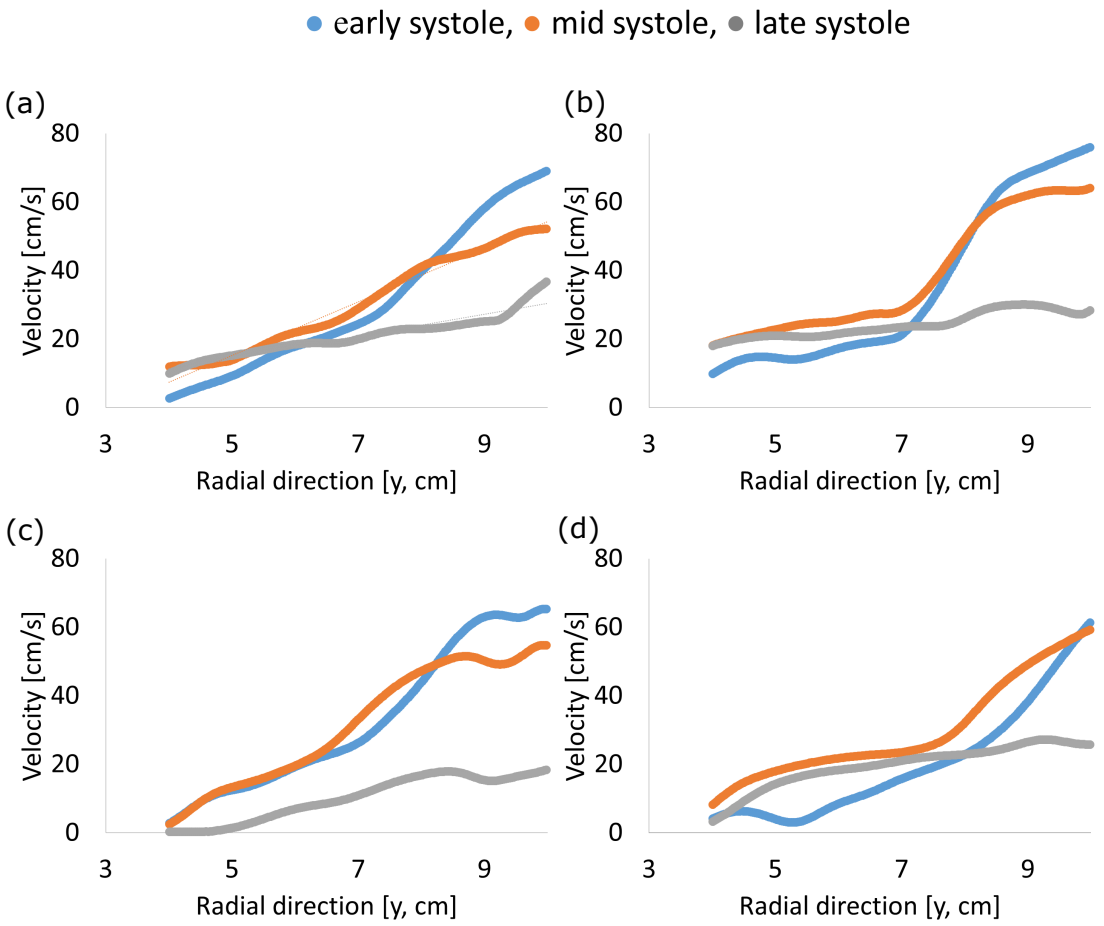

FIGURE 5.11: The blood flow velocity distribution curve (VDC) on the MFAL in healthy volunteers. VDC started in the apex, gradually increased in the center and steeply increased in the base of LV in healthy LV. VDC in the base of LV show the highest velocity magnitude during early systole phase in example of (a) volunteer 1, (b) volunteer 2, (c) volunteer 3, and (d) volunteer 4.

Table 5.2 showed a comparison of gradient and slope angle in healthy volunteers and AS patients during early, mid and late systoles. The maximum slope of the blood flow velocity distribution curve on MFAL was compared in healthy, patients with AS and patients suspected MI. The maximum slope was significantly larger in the healthy LV indicating normal cardiac function (healthy: 10.91 ± 2.16 (early), 8.81 ± 0.72 (mid), 2.97 ± 0.69 (late), $p<0.0001$ vs. AS: 8.34 ± 2.20 (early), 9.09 ± 0.96 (mid), 5.40 ± 2.42 (late), $p=0.0028$ vs. MI: 7.44 ± 3.11 (early), 6.86 ± 2.47 (mid), and 4.80 ± 2.71 (late), $p=0.4055$). Moreover, the maximum slope angle of

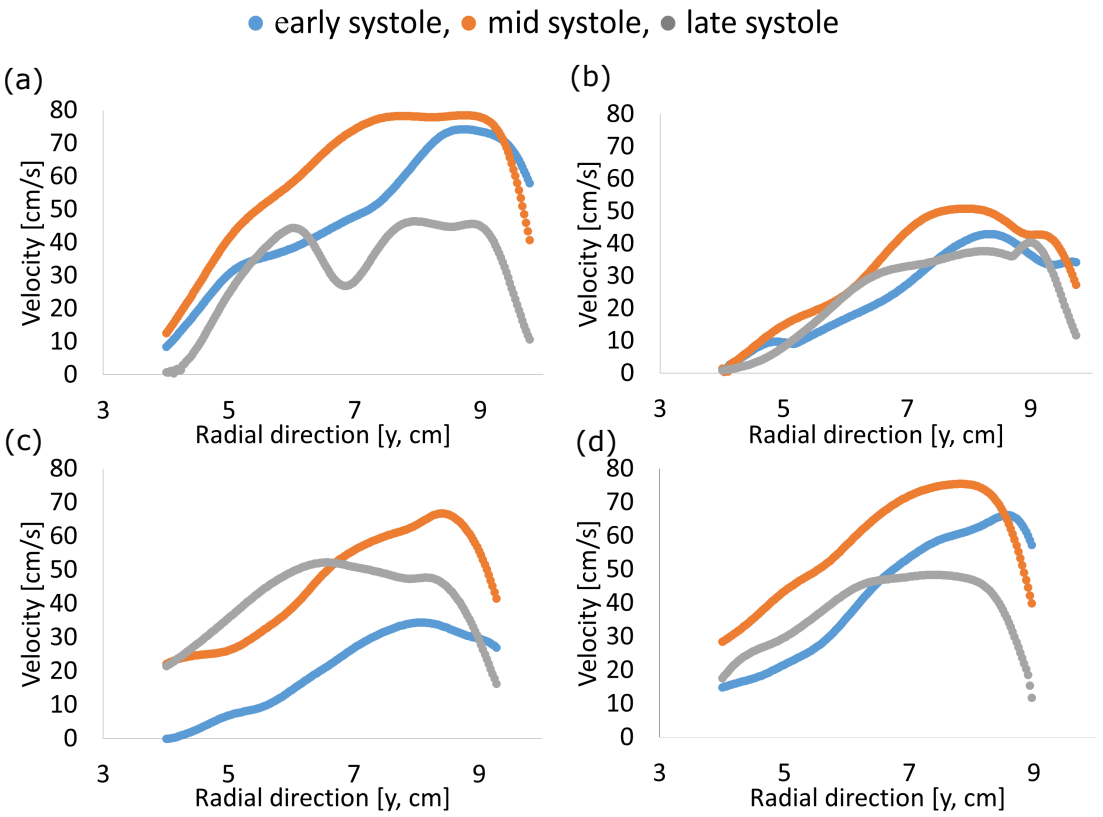

FIGURE 5.12: The blood flow velocity distribution curve (VDC) on the MFAL in aortic stenosis (AS) patients. VDC started in the apex and was downward convex. The highest velocity magnitude during mid systole phase in the base LV. In late systole, the flow linearly toward LV outflow example of (a) patient 1, (b) patient 2, (c) patient 3, and (d) patient 4.

TABLE 5.2: Comparison of gradient and slope angle of healthy volunteers, aortic stenosis and myocardial infarction patients

Group	Phase	Gradient	p-value	Slope angle	p-value
`healthy`	early	10.91 ± 2.16		84.57 ± 1.29	
	mid	8.81 ± 0.72	< 0.0001	83.49 ± 0.55	0.000206
	late	2.97 ± 0.69		70.61 ± 5.17	
`AS`	early	8.34 ± 2.20		82.75 ± 1.84	
	mid	9.09 ± 0.96	0.0028	83.64 ± 0.68	0.0198
	late	5.40 ± 2.42		76.86 ± 8.04	
`MI`	early	7.44 ± 3.11		81.10 ± 4.26	
	mid	6.86 ± 2.47	0.4055	81.07 ± 3.02	0.3903
	late	4.80 ± 2.71		71.33 ± 18.34	

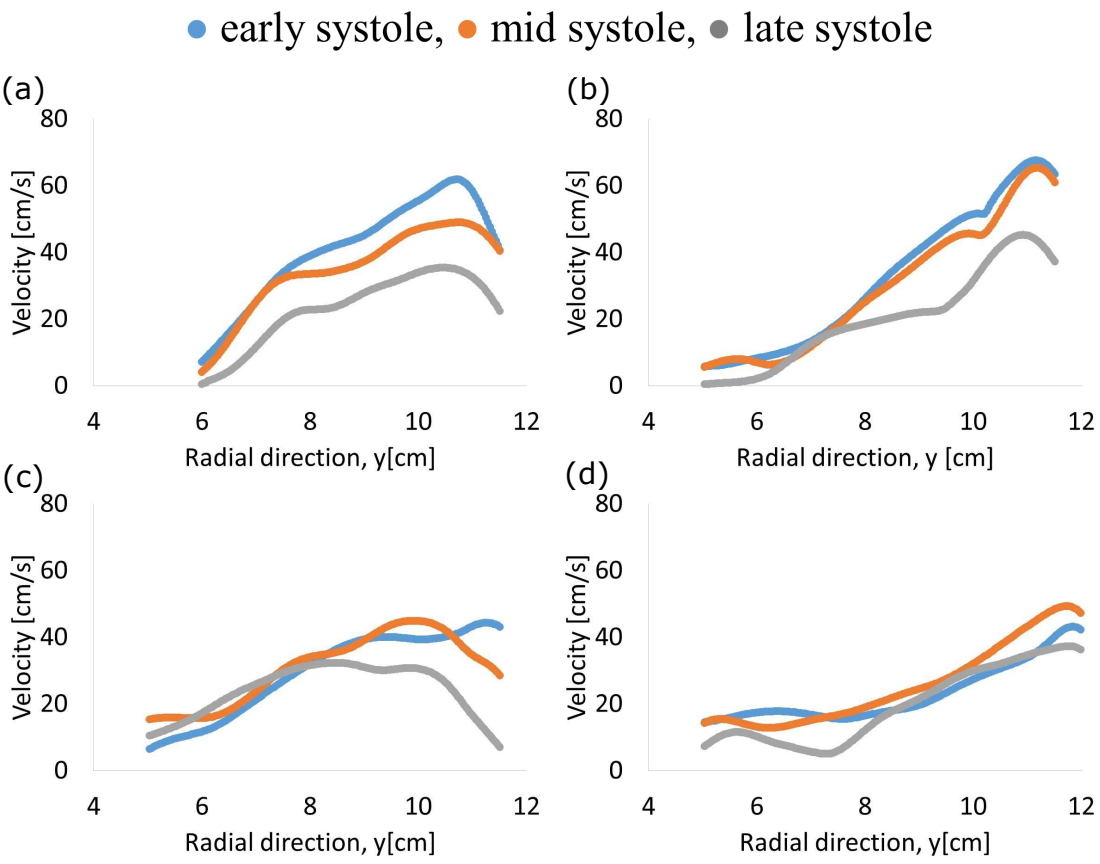

FIGURE 5.13: The blood flow velocity distribution curve (VDC) on the MFAL in myocardial infarction (MI) patients. The VDC example of (a) patient 1, (b) patient 2, (c) patient 3, and (d) patient 4.

the MFAL to apex showed a significant difference between healthy volunteers, AS patients and MI patients (the maximum slope of the MFAL: healthy 84.57 $\pm$ 1.29, AS 83.64 $\pm$ 0.68, MI 81.10 $\pm$ 4.26).

We observed the data means of several groups differentiate of cardiac cycle and to made inferences using ANOVA single factor analyzed. In this study, The result showed $p < 0.05$, then we accepted that the gradients and slope angle were significantly different in healthy volunteers and AS patients except in MI patients during late systoles.

5.4 Conclusion

In summary, the 2D velocity vectors of blood flow were visualized, and the LV vortex parameters were quantified by EDG method using CDE images in healthy, patients with AS and patients suspected MI. A powerful blood flow pushed and increased the speed of circulation of the vortex. Consequently, vortices were generated from LV basal to LV apex with a brief appearance of the vortex in the LV outflow tract formed blood flow clockwise in the healthy participants and the vortices were located at the center of the LV during the cardiac cycle and flow direction was incoherent.

The 2D velocity vectors of blood flow were visualized, and the vortices during IVC were represented. we described several LV vortex parameters responsible for quantitative analysis such as vortex strength, vortex shape (sphericity index, I_s) and Reynolds number. Vortex parameters such as vortex strength, vortex shape and Reynolds number showed a significant difference between healthy participants, AS patients and MI patients. The data of this study showed the differences in quantitative vortex parameter in all participants. The vortex of the healthy LV groups was typically ellipse than AS and MI. Therefore, these quantitative and non-invasive vortex measurements are feasible and distinguishable between healthy as normal case, AS and MI as abnormal cases of LV function.

MFAL is defined as velocity distribution on the y-axis with estimating the maximum and mean velocities. [49, 67] argue that the cross-sectional mean velocity is an essential variable in open-channel hydraulic and the relation between mean and

maximum speeds in a natural river even in a large river such as the Mississippi river is found the maximum velocity occurs as much as one-third of the water depth below the water surface. This result may relate to the location of MFAL below the blood surface when we assume that the flow from apex of LV to the aorta through LV outflow is open-channel flow, and the surface is the ventricular wall.

A zero-vorticity point can be used to help recognize MFAL. The study showed MFAL path coincides with the irrotational flow path, $\omega = 0$. This physical phenomenon can be analyzed as a linear stability [68]. However, this study is finite to the correlation zero vorticity and MFAL in LV systole function. Furthermore, LV diastole should be evaluated with these parameters.

The blood velocity distribution curve on the MFAL showed a significant difference in healthy, AS and MI. The velocity distribution curve gradually increased nearly LV outflow in healthy and moved linear or decreased nearly the LV outflow in AS and also the MFAL started from the center of LV, and the flow linearly increased toward to LV outflow in MI patients. Accordingly, acceleration is suspected caused by alteration direction of the intraventricular blood flow, the transmitting process of the ejection force produced by the wall contraction. In contrast, the gradients and slope angle of blood flow were not significantly different during systoles. Limited of the sample size probably cause difficulties of measurement the correlation gradient of blood flow and limitation of frame rate cause error to determine the phase of the cardiac cycle through the graphic outline of the heart movement, especially in patients with heart rate changing significantly.

The EDG method provides additional insights about vortex flow and MFAL to assess LV function and may be an essential tool for quantitative assessment of cardiac blood flow in the future.

Chapter 6

Conclusion

In this dissertation, I have discussed the two-dimensional blood flow velocity vectors, particle image velocimetry validation studies, and application for the clinical cardiography. We have three main purposes of the dissertation. Correspondingly, the conclusions of this dissertation can be summarized as follows.

6.1 Summary and Clinical Impact

The present study investigated quantitative information on blood flow in LV during the cardiac cycle. There are three steps to assess the LV function: (1) image acquisition, (2) image processing, and (3) image analysis. All volunteers underwent CDE using the iE33 ultrasound system (Philips Ultrasound, Bothell, WA, USA), then the CDE images were processed and analyzed using MATLAB R2016b (Mathworks, Natick, MA, USA).

Image processing is performed to reconstructed CDE image, selection area of blood flow based on biologically motivated, and to eliminate ambiguity in the intrinsic magnitude and direction for Doppler measurement. Physiological flow velocities sometimes exceed low and high Nyquist velocity, resulting in aliasing. Therefore the scale and direction are displayed incorrectly when the blood flow rate increase and exceeds the Nyquist limit. De-aliasing comes as a solution of the ambiguous estimates speed and direction from the raw measurement. Then Median and Gaussian filterings are robust concerning missing and additional data.

CDE provides information on 1D of blood flow far away or approaching the transducer beam. Because of this, this study proposes the two-dimensional blood flow. Investigation of two-dimensional flow and hemodynamic parameter with applying fluid dynamic theory to CDE. This method is called echodynamography (EDG). EDG is a computational method that estimated and visualized blood flow velocity distribution and hemodynamic parameters such as vortex, vorticity, and MFAL.

Two-dimensional blood flow algorithm is required validation if applied to human cardiac flow function. The validation of EDG was investigated in comparison to PIV measurements using an LV phantom that enables optical observations of flow in the same phase and cross-section. The results were not significantly different between EDG and PIV in visual representation. These findings on the EDG validation appropriated for estimating and visualizing velocity vectors in clinical studies since higher measurement accuracy and reliability.

Two-dimensional blood flow in healthy, MI, and AS patients successfully were estimated, visualized, and quantitated the hemodynamic parameter that may contribute to the practical and clinical diagnosis of LV assessments.

6.2 Limitations and Future Work

The EDG method has some limitations. Firstly, EDG can be applied only in the offline analysis and analyzed frame by frame, which is time-consuming. Secondly, EDG is estimated from two-dimensional distribution, complicated three-dimensional flow occurs, and two-dimensional flow assumption could not validate overall. Thirdly, the use of color Doppler as a data source, which requires manual correction of aliasing for velocities exceeding the Nyquist velocity. Fourthly, validation EDG algorithm by comparing data between original PIV and virtual color Doppler obtained by PIV could not replace the whole if using original CDE. Then, the number of cases evaluated was small, exceptionally healthy, MI, and AS patients.

Further studies involving larger samples are needed to confirm the results of the current research, to improve the EDG algorithm, and these limitations could be overcome in the future. EDG method provides additional insights for representing a cardiac function and thus, the clinical implications of vortex, vorticity, and MFAL warrant further investigation.

6.3 Publication List

Doctoral Program, Graduate School of Biomedical Engineering, Tohoku University

1. **Oktamuliani, Sri**, Kaoru Hasegawa, and Yoshifumi Saijo."Left Ventricular Vortices in Myocardial Infarction Observed with Echodynamography." Accepted for publication in Conference proceedings of IEEE EMBC, 2019.

2. **Oktamuliani, Sri**, Kaoru Hasegawa, and Yoshifumi Saijo. "Blood Flow Patterns in The Left Ventricle by Echodynamography Method." Conference proceedings of IEEE International Conference on Orange Technologies (ICOT), 2018. DOI: 10.1109/ICOT.2018.8705826.

3. **Oktamuliani, Sri**, Kaoru Hasegawa, and Yoshifumi Saijo. "Correction of Aliasing in Color Doppler Echocardiography Based on Image Processing Technique in Echodynamography." Proceedings of the 3rd International Conference on Biomedical Signal and Image Processing. ACM, 2018. ISBN: 978-1-4503-6436-2. DOI:10.1145/3278229.3278233.

4. Minagawa T, **Oktamuliani, S**, Kurokawa T, Nakajima H, Hasegawa K, Matsuoka T, Shimizu T, Miura M, Ohara T, Kawamoto S. "Left Ventricular Blood Flow Dynamics In Aortic Stenosis Before And After Aortic Valve Replacement." Conference Proceedings of 40th IEEE Engineering in Medicine and Biology Society (EMBC). 3177-3180, 2018. DOI: 10.1109/EMBC.2018.8512954.

5. **Oktamuliani, Sri**, Yoshifumi Saijo, and Kaoru Hasegawa. "Evaluation of blood flow dynamics in healthy and myocardial infarction hearts using Echo-dynamography." Proceedings of Meetings on Acoustics 6ICU. Vol. 32. No. 1. ASA, 2017. Proc. Mtgs. Acoust. 32, 020007 (2017); DOI:10.1121/2.0000716.

Master Program, Department of Physics, Institut Teknologi bandung

1. **Oktamuliani, Sri**, and Zaki Su'ud. "Design study of lead bismuth cooled fast reactors and capability of natural circulation." AIP Conference Proceedings. Vol. 1677. No. 1. AIP Publishing, 2015.

Undergraduate Program, Department of Physics, Universitas Andalas

1. **Oktamuliani, Sri**, and Dian Fitriyani. "Optimasi Ukuran Teras Dan Daya Termal Terhadap Tingkat Sirkulasi Alamiah Bahan Pendingin Pb-bi Pada Reaktor Cepat." JURNAL ILMU FISIKA— UNIVERSITAS ANDALAS 4.2 (2012): 53-61.

References

[1] John Enderle and Joseph Bronzino. *Introduction to biomedical engineering*. Academic press, 2012.

[2] World Health Organization. The top 10 causes of death, 24.

[3] Yasuhiko Sakata and Hiroaki Shimokawa. Epidemiology of heart failure in asia. *Circulation Journal*, pages CJ–13, 2013.

[4] Yuji Okura, Mahmoud M Ramadan, Yukiko Ohno, Wataru Mitsuma, Komei Tanaka, Masahiro Ito, Keisuke Suzuki, Naohito Tanabe, Makoto Kodama, and Yoshifusa Aizawa. Impending epidemic. *Circulation Journal*, 72(3):489–491, 2008.

[5] Patrizio Lancellotti, Vuyisile T Nkomo, Luigi P Badano, Jutta Bergler-Klein, Jan Bogaert, Laurent Davin, Bernard Cosyns, Philippe Coucke, Raluca Dulgheru, Thor Edvardsen, et al. Expert consensus for multi-modality imaging evaluation of cardiovascular complications of radiotherapy in adults: a report from the european association of cardiovascular imaging and the american society of echocardiography. *European Heart Journal–Cardiovascular Imaging*, 14(8):721–740, 2013.

[6] Rajesh Puranik, Vivek Muthurangu, David S Celermajer, and Andrew M Taylor. Congenital heart disease and multi-modality imaging. *Heart, Lung and Circulation*, 19(3):133–144, 2010.

[7] Francesca Romana Pluchinotta and Massimo Lombardi. Cardiac magnetic resonance. In *Atlas of Cardiac Catheterization for Congenital Heart Disease*, pages 339–349. Springer, 2019.

[8] Michael Markl. Techniques in the assessment of cardiovascular blood flow and velocity. In *Cardiovascular Magnetic Resonance Imaging*, pages 113–125. Springer, 2019.

[9] Stanley J Goldberg, Hugh D Allen, Gerald R Marx, and CJ Flinn. *Doppler echocardiography*. Lea & Febiger Philadelphia, 1985.

[10] James V Chapman and George R Sutherland. *The Noninvasive Evaluation of Hemodynamics in Congenital Heart Disease: Doppler Ultrasound Applications in the Adult and Pediatric Patient with Congenital Heart Disease*, volume 114. Springer Science & Business Media, 2012.

[11] Markus Raffel, Christian E Willert, Fulvio Scarano, Christian J Kähler, Steve T Wereley, and Jürgen Kompenhans. *Particle image velocimetry: a practical guide*. Springer, 2018.

[12] Chouchou Tang, Yizhong Zhu, Jing Zhang, Chengcheng Niu, Dan Liu, Yacong Liao, Lijun Zhu, and Qinghai Peng. Analysis of left ventricular fluid dynamics in dilated cardiomyopathy by echocardiographic particle image velocimetry. *Echocardiography*, 35(1):56–63, 2018.

[13] Brett A Meyers, Craig J Goergen, and Pavlos P Vlachos. Development and validation of a phase-filtered moving ensemble correlation for echocardiographic particle image velocimetry. *Ultrasound in Medicine & Biology*, 44 (2):477–488, 2018.

[14] Jing Lu, Wenhua Li, Yu Zhong, Anguo Luo, Shenghua Xie, and Lixue Yin. Intuitive visualization and quantification of intraventricular convection in acute ischemic left ventricular failure during early diastole using color doppler-based echocardiographic vector flow mapping. *The International Journal of Cardiovascular Imaging*, 28(5):1035–1047, 2012.

[15] Iman Borazjani, John Westerdale, Eileen M McMahon, Prathish K Rajaraman, Jeffrey J Heys, and Marek Belohlavek. Left ventricular flow analysis: recent advances in numerical methods and applications in cardiac ultrasound. *Computational and Mathematical Methods in Medicine*, 2013, 2013.

[16] Tokuhisa Uejima, Akira Koike, Hitoshi Sawada, Tadanori Aizawa, Shigeo Ohtsuki, Motonao Tanaka, Tetsushi Furukawa, and Alan G Fraser. A new echocardiographic method for identifying vortex flow in the left ventricle: numerical validation. *Ultrasound in Medicine & Biology*, 36(5):772–788, 2010.

[17] Zhang Haibin, Zhang Jun, Zhu Xiaoxing, Chen Lulu, Liu Liwen, Duan Yunyan, Yu Ming, Zhou Xiaodong, Zhu Ting, Zhu Miaozhang, and Li Hongling.

The left ventricular intracavitary vortex during the isovolumic contraction period as detected by vector flow mapping. *Echocardiography*, 29(5):579–587, 2011.

[18] D. Garcia, J. C. del Alamo, D. Tanne, R. Yotti, C. Cortina, É. Bertrand, J. C. Antoranz, E. Perez-David, R. Rieu, F. Fernandez-Aviles, and J. Bermejo. Two-dimensional intraventricular flow mapping by digital processing conventional color-doppler echocardiography images. *IEEE Transactions on Medical Imaging*, 29(10):1701–1713, Oct 2010. ISSN 0278-0062. doi: 10.1109/TMI.2010.2049656.

[19] Motonao Tanaka, Tsuguya Sakamoto, Shigeo Sugawara, Hiroyuki Nakajima, Takeyoshi Kameyama, Yoshiaki Katahira, Shigeo Ohtsuki, and Hiroshi Kanai. Spiral systolic blood flow in the ascending aorta and aortic arch analyzed by echo-dynamography. *Journal of Cardiology*, 56(1):97–110, 2010.

[20] Motonao Tanaka, Tsuguya Sakamoto, Shigeo Sugawara, Hiroyuki Nakajima, Takeyoshi Kameyama, Haruna Tabuchi, Yoshiaki Katahira, Shigeo Ohtsuki, and Hiroshi Kanai. Physiological basis and clinical significance of left ventricular suction studied using echo-dynamography. *Journal of Cardiology*, 58 (3):232–244, 2011.

[21] Takanori Kojima, Takeyoshi Kameyama, Hiroyuki Nakajima, Elena Khmyrova, Takafumi Kurokawa, and Yoshifumi Saijo. Evaluation of vortex flow in left ventricle by echo-dynamography and phase contrast magnetic resonance angiography. In *Engineering in Medicine and Biology Society (EMBC), 2012 Annual International Conference of the IEEE*, pages 2676–2679. IEEE, 2012.

[22] James V Chapman and A Sgalambro. *Basic Concepts in Doppler Echocardiography: Methods of clinical applications based on a multi-modality Doppler approach*, volume 73. Springer Science & Business Media, 2012.

[23] Catherine M Otto. *Textbook of Clinical Echocardiography E-Book*. Elsevier Health Sciences, 2013.

[24] Warren J Manning. Asymptomatic aortic stenosis in the elderly: a clinical review. *Jama*, 310(14):1490–1497, 2013.

[25] Helmut Baumgartner, Judy Hung, Javier Bermejo, John B Chambers, Arturo Evangelista, Brian P Griffin, Bernard Iung, Catherine M Otto, Patricia A Pellikka, and Miguel Quiñones. Echocardiographic assessment of valve stenosis:

Eae/ase recommendations for clinical practice. *Journal of the American Society of Echocardiography*, 22(1):1–23, 2009.

[26] Maria Olszowska. Pathogenesis and pathophysiology of aortic valve stenosis in adults. *Pol Arch Med Wewn*, 121(11):409–413, 2011.

[27] Heinz Handels, Sven Mersmann, Christoph Palm, Thomas Tolxdorff, Gudrun Wagenknecht, Thomas Wittenberg, et al. Viewpoints on medical image processing: from science to application. *Current Medical Imaging Reviews*, 9(2): 79–88, 2013.

[28] Sri Oktamuliani, Kaoru Hasegawa, and Yoshifumi Saijo. Correction of aliasing in color doppler echocardiography based on image processing technique in echodynamography. In *Proceedings of the 3rd International Conference on Biomedical Signal and Image Processing*, pages 1–5. ACM, 2018.

[29] Sri Oktamuliani, Kaoru Hasegawa, and Yoshifumi Saijo. Blood flow patterns in the left ventricle by echodynamography method. In *2018 International Conference on Orange Technologies (ICOT)*, pages 1–3. IEEE, 2018.

[30] DJA Price, DR Wallbridge, and MJ Stewart. Tissue doppler imaging: current and potential clinical applications. *Heart*, 84(suppl 2):ii11–ii18, 2000.

[31] Geu-Ru Hong, Minji Kim, Gianni Pedrizzetti, and Mani A Vannan. Current clinical application of intracardiac flow analysis using echocardiography. *Journal of Cardiovascular Ultrasound*, 21(4):155–162, 2013.

[32] Shigeo Ohtsuki and Motonao Tanaka. Doppler pressure field deduced from the doppler velocity field in an observation plane in a fluid. *Ultrasound in Medicine and Biology*, 29(10):1431–1438, 2003.

[33] Shigeo Ohtsuki and Motonao Tanaka. The flow velocity distribution from the doppler information on a plane in three-dimensional flow. *Journal of Visualization*, 9(1):69–82, 2006.

[34] Roger Temam. *Navier-Stokes equations: theory and numerical analysis*, volume 343. American Mathematical Soc., 2001.

[35] D Kumar, R Vinoth, Raviraj Adhikari, and Vijay Shankar. Non-newtonian and newtonian blood flow in human aorta: A transient analysis. *Biomedical Research*, 28(7):3194–3194, 2017.

[36] Arash Kheradvar, Helene Houle, Gianni Pedrizzetti, Giovanni Tonti, Todd Belcik, Muhammad Ashraf, Jonathan R Lindner, Morteza Gharib, and David Sahn. Echocardiographic particle image velocimetry: a novel technique for quantification of left ventricular blood vorticity pattern. *Journal of the American Society of Echocardiography*, 23(1):86–94, 2010.

[37] Gianni Pedrizzetti, Federico Domenichini, and Giovanni Tonti. On the left ventricular vortex reversal after mitral valve replacement. *Annals of Biomedical Engineering*, 38(3):769–73, 2010.

[38] Kyu-Hwan Park, Jang-Won Son, Won-Jong Park, Sang-Hee Lee, Ung Kim, Jong-Seon Park, Dong-Gu Shin, Young-Jo Kim, Jung-Hyun Choi, Helene Houle, Mani A. Vannan, and Geu-Ru Hong. Characterization of the left atrial vortex flow by two-dimensional transesophageal contrast echocardiography using particle image velocimetry. *Ultrasound in Medicine & Biology*, 39(1): 62–71, 2013.

[39] Daniel Rodríguez Muñoz, José Luis Moya Mur, Covadonga Fernández-Golfín, Derly Carlos Becker Filho, Ariana González Gómez, Sara Fernández Santos, Carla Lázaro Rivera, Luis Miguel Rincón Díaz, Eduardo Casas Rojo, and José Luis Zamorano Gómez. Left ventricular vortices as observed by vector flow mapping: main determinants and their relation to left ventricular filling. *Echocardiography*, 32(1):96–105, 2015.

[40] Kondo Claude Assi, Etienne Gay, Christophe Chnafa, Simon Mendez, Franck Nicoud, Juan FPJ Abascal, Pierre Lantelme, François Tournoux, and Damien Garcia. Intraventricular vector flow mapping—a doppler-based regularized problem with automatic model selection. *Physics in Medicine & Biology*, 62 (17):7131, 2017.

[41] Sri Oktamuliani, Yoshifumi Saijo, and Kaoru Hasegawa. Evaluation of blood flow dynamics in healthy and myocardial infarction hearts using echodynamography. In *Proceedings of Meetings on Acoustics 6ICU*, volume 32, page 020007. ASA, 2017.

[42] Geu-Ru Hong, Gianni Pedrizzetti, Giovanni Tonti, Peng Li, Zhao Wei, Jin Kyung Kim, Abinav Baweja, Shizhen Liu, Namsik Chung, Helene Houle, et al. Characterization and quantification of vortex flow in the human left ventricle by contrast echocardiography using vector particle image velocimetry. *JACC: Cardiovascular Imaging*, 1(6):705–717, 2008.

[43] M Shimizu, R Tanaka, R Fukushima, L Hamabe, and N Sasaki. Evaluation of diastolic blood flow dynamic of the left ventricle in dogs with mitral valve regurgitation using vector flow mapping. *Iranian Journal of Veterinary Research*, 15(2):93–98, 2014.

[44] JW Heyt and JM Diaz. Pressure drop in flat-oval spiral air duct. *ASHRAE Transactions*, 81(Part 2):221–230, 1975.

[45] John Happel and Howard Brenner. *Low Reynolds number hydrodynamics: with special applications to particulate media*, volume 1. Springer Science & Business Media, 2012.

[46] Jie-Zhi Wu, Hui-Yang Ma, and M-D Zhou. *Vorticity and vortex dynamics*. Springer Science & Business Media, 2007.

[47] Motonao Tanaka, Tsuguya Sakamoto, Shigeo Sugawara, Hiroyuki Nakajima, Yoshiaki Katahira, Shigeo Ohtsuki, and Hiroshi Kanai. Blood flow structure and dynamics, and ejection mechanism in the left ventricle: analysis using echo-dynamography. *Journal of Cardiology*, 52(2):86–101, 2008.

[48] Hiroyuki Nakajima, Shigeo Sugawara, Takeyoshi Kameyama, Haruna Tabuchi, Shigeo Ohtsuki, Motonao Tanaka, and Yoshifumi Saijo. Location of flow axis line in the left ventricle and its interaction with local myocardial motion. *Journal of Echocardiography*, 9(1):24–29, 2011.

[49] Chao-Lin Chiu and Chairil A Abidin Said. Maximum and mean velocities and entropy in open-channel flow. *Journal of Hydraulic Engineering*, 121(1): 26–35, 1995.

[50] Takanori Kojima, Aiko Omori, Hiroyuki Nakajima, Takafumi Kurokawa, Takeyoshi Kameyama, and Yoshifumi Saijo. Validation of echo-dynamography by virtual color doppler echocardiography generated from phase contrast magnetic resonance angiography datasets. In *Engineering in Medicine and Biology Society (EMBC), 2013 35th Annual International Conference of the IEEE*, pages 105–108. IEEE, 2013.

[51] Peter D Gatehouse, Jennifer Keegan, Lindsey A Crowe, Sharmeen Masood, Raad H Mohiaddin, Karl-Friedrich Kreitner, and David N Firmin. Applications of phase-contrast flow and velocity imaging in cardiovascular mri. *European radiology*, 15(10):2172–2184, 2005.

[52] Petter Dyverfeldt, John-Peder Escobar Kvitting, Andreas Sigfridsson, Jan Engvall, Ann F Bolger, and Tino Ebbers. Assessment of fluctuating velocities in disturbed cardiovascular blood flow: In vivo feasibility of generalized phase-contrast mri. *Journal of Magnetic Resonance Imaging*, 28(3):655–663, 2008.

[53] Anders Nilsson, Karin Markenroth Bloch, Johannes Töger, Einar Heiberg, and Freddy Ståhlberg. Accuracy of four-dimensional phase-contrast velocity mapping for blood flow visualizations: a phantom study. *Acta Radiologica*, 54(6):663–671, 2013.

[54] Michelle Borkin, Krzysztof Gajos, Amanda Peters, Dimitrios Mitsouras, Simone Melchionna, Frank Rybicki, Charles Feldman, and Hanspeter Pfister. Evaluation of artery visualizations for heart disease diagnosis. *IEEE Transactions on Visualization and Computer Graphics*, 17(12):2479–2488, 2011.

[55] Charles A Taylor, Timothy A Fonte, and James K Min. Computational fluid dynamics applied to cardiac computed tomography for noninvasive quantification of fractional flow reserve: scientific basis. *Journal of the American College of Cardiology*, 61(22):2233–2241, 2013.

[56] Radoslav Kaminsky, K Dumont, H Weber, M Schroll, and Pascal Verdonck. Piv validation of blood-heart valve leaflet interaction modelling. *The International Journal of Artificial Organs*, 30(7):640–648, 2007.

[57] C Brossard, JC Monnier, P Barricau, F-XAVIER Vandernoot, Y Le Sant, F Champagnat, and G Le Besnerais. Principles and applications of particle image velocimetry. *AerospaceLab*, (1):p–1, 2009.

[58] James R Blake, William J Easson, and Peter R Hoskins. A dual-phantom system for validation of velocity measurements in stenosis models under steady flow. *Ultrasound in Medicine & Biology*, 35(9):1510–1524, 2009.

[59] Suong-Hyu Hyon and Yoshito Ikada. Porous and transparent poly (vinyl alcohol) gel and method of manufacturing the same, May 5 1987. US Patent 4,663,358.

[60] S-H Hyon, W-I Cha, and Y Ikada. Preparation of transparent poly (vinyl alcohol) hydrogel. *Polymer Bulletin*, 22(2):119–122, 1989.

[61] Manuel R Vegas and Jose L Martin Del Yerro. Stiffness, compliance, resilience, and creep deformation: understanding implant-soft tissue dynamics in the

augmented breast: fundamentals based on materials science. *Aesthetic Plastic Surgery*, 37(5):922–930, 2013.

[62] Toshinosuke Akutsu, Ryota Imai, and Yuuki Deguchi. Effect of the flow field of mechanical bileaflet mitral prostheses on valve closing. *Journal of Artificial Organs*, 8(3):161–170, 2005.

[63] Réka Faludi, Mariola Szulik, Jan D'hooge, Paul Herijgers, Frank Rademakers, Gianni Pedrizzetti, and Jens-Uwe Voigt. Left ventricular flow patterns in healthy subjects and patients with prosthetic mitral valves: an in vivo study using echocardiographic particle image velocimetry. *The Journal of Thoracic and Cardiovascular Surgery*, 139(6):1501–1510, 2010.

[64] Tadanori Minagawa, Yoshifumi Saijo, Sri Oktamuliani, Takafumi Kurokawa, Hiroyuki Nakajima, Kaoru Hasegawa, Takayuki Matsuoka, Takuya Shimizu, Makoto Miura, Takahiro Ohara, et al. Left ventricular blood flow dynamics in aortic stenosis before and after aortic valve replacement. In *2018 40th Annual International Conference of the IEEE Engineering in Medicine and Biology Society (EMBC)*, pages 3177–3180. IEEE, 2018.

[65] Satoshi Numata, Keiichi Itatani, Keiichi Kanda, Kiyoshi Doi, Sachiko Yamazaki, Kazuki Morimoto, Kaichiro Manabe, Koki Ikemoto, and Hitoshi Yaku. Blood flow analysis of the aortic arch using computational fluid dynamics. *European Journal of Cardio-Thoracic Surgery*, 49(6):1578–1585, 2016.

[66] Vijay Govindarajan, John Mousel, HS Udaykumar, Sarah C Vigmostad, David D McPherson, Hyunggun Kim, and Krishnan B Chandran. Synergy between diastolic mitral valve function and left ventricular flow aids in valve closure and blood transport during systole. *Scientific reports*, 8(1):6187, 2018.

[67] Renjie Xia. Relation between mean and maximum velocities in a natural river. *Journal of Hydraulic Engineering*, 123(8):720–723, 1997.

[68] Yu-Hau Tseng and Andrea Prosperetti. Local interfacial stability near a zero vorticity point. *Journal of Fluid Mechanics*, 776:5–36, 2015.

Institutional Review Board

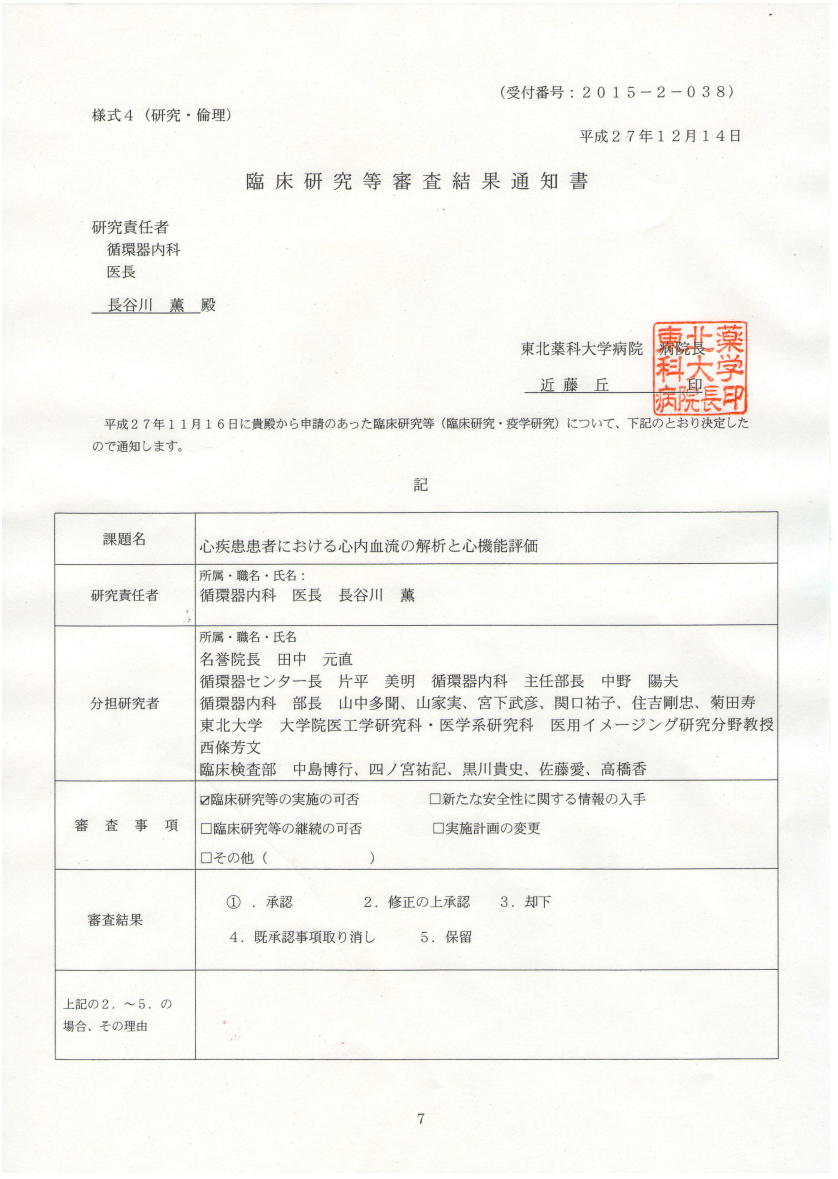

（受付番号：２０１５－２－０３８）

様式４（研究・倫理）

平成２７年１２月１４日

臨床研究等審査結果通知書

研究責任者
循環器内科
医長

長谷川　薫　殿

東北薬科大学病院　病院長
近藤　丘　印

平成２７年１１月１６日に貴殿から申請のあった臨床研究等（臨床研究・疫学研究）について、下記のとおり決定したので通知します。

記

課題名	心疾患患者における心内血流の解析と心機能評価
研究責任者	所属・職名・氏名： 循環器内科　医長　長谷川　薫
分担研究者	所属・職名・氏名 名誉院長　田中　元直 循環器センター長　片平　美明　循環器内科　主任部長　中野　陽夫 循環器内科　部長　山中多聞、山家実、宮下武彦、関口祐子、住吉剛忠、菊田寿 東北大学　大学院医工学研究科・医学系研究科　医用イメージング研究分野教授 西條芳文 臨床検査部　中島博行、四ノ宮祐記、黒川貴史、佐藤愛、高橋香
審査事項	☑臨床研究等の実施の可否　□新たな安全性に関する情報の入手 □臨床研究等の継続の可否　□実施計画の変更 □その他（　　）
審査結果	①．承認　2．修正の上承認　3．却下 4．既承認事項取り消し　5．保留
上記の２．～５．の場合、その理由	

7

Publication File